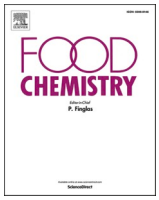
Food Chemistry 476 (2025) 143427



Contents lists available at ScienceDirect

Food Chemistry

journal homepage: www.elsevier.com/locate/foodchem





Green synthesis of gold nanoparticles from pomegranate juice ascertained by a combined approach based on MALDI FT-ICR MS and LC-ESI-MS/MS

Maria Assunta Acquavia [a,*], Jennifer Gubitosa [b,c], Vito Rizzi [b], Pinalysa Cosma [b], Carmine Gaeta [d], Patrizia Iannece [d], Paolo Della Sala [d], Antonio Guerrieri [a], Carmen Tesoro [a], Rosanna Ciriello [a], Filomena Lelario [a], Emanuela Gregori [e], Paola Montoro [f], Angela Di Capua [a], Giuliana Bianco [a]

[a] Università degli Studi della Basilicata, Dipartimento di Scienze di Base e Applicate, Via dell'Ateneo Lucano 10, Potenza, Italy
[b] Università degli Studi "Aldo Moro" di Bari, Dipartimento di Chimica, Via Orabona, 4, Bari, Italy
[c] Consiglio Nazionale delle Ricerche, Istituto di Nanotecnologia (CNR-NANOTEC), Sede Secondaria di Bari, c/o Dipartimento di Chimica, Università degli Studi di Bari "Aldo Moro", 70126 Bari, Italy
[d] Università degli Studi di Salerno, Dipartimento di Chimica e Biologia, Via Giovanni Paolo II 132, Fisciano, Italy
[e] Istituto Superiore di Sanità, Dept. Food Safety, Nutrition and Veterinary Public Health, Viale Regina Elena, 299, 00161 Rome, Italy
[f] Università degli Studi di Salerno, Dipartimento di Farmacia, Via Giovanni Paolo II 132, Fisciano, Italy

ARTICLE INFO

Keywords:
Pomegranate juice
Au nanoparticles
MALDI FT-ICR MS
Van Krevelen
Phenols
LC-MS/MS

ABSTRACT

This research employs advanced analytical techniques to explore the specific roles of Pomegranate Juice (PJ) phytochemicals in both the reduction and stabilization of gold nanoparticles (AuNPs) obtained by means of juice from wasted fruits. A level 3 for classes annotation, used for MALDI FT ICR-MS data, was useful to provide an immediate visualization of the main involved metabolites in AuNPs synthesis, through van Krevelen diagrams. More than 25 elemental formulae containing at least one Au atom were assigned to AuNPs sample, confirming the formation of organogold complexes. LC-MS/MS analysis allowed a level 2 annotation of polyphenols and carbohydrates involved in metal reduction and AuNPs surface coating. This work highlights the potential of PJ in green nanoparticles synthesis, providing insights into the bioactive compounds responsible for the tunable characteristics of AuNPs.

1. Introduction

Pomegranate (*Punica granatum L.*) is currently accepted as one of the fruits with a prominent antioxidant activity, due to its high content of phenolic compounds (Akhtar, Ismail, Fraternale, & Sestili, 2015; Çam & Hişil, 2010; Fischer, Carle, & Kammerer, 2011; Kalaycıoğlu & Erim, 2017; Qu, Breksa, Pan, & Ma, 2012; Singh, Singh, Kaur, & Singh, 2018). The global demand for this fruit has increased and *Punica granatum* is now harvested in many parts of the world. Pomegranate juices (PJ) show high nutritional values that justify their addition in several other food products, like jams or yogurts, also as a novel flavor for new product development and line extensions (Krueger, 2012). Pomegranate fruits and derived juices include a wide range of metabolites contributing to positive effects on health. Besides phenolics, PJ encompasses sugars, mainly glucose, fructose and sucrose, alongside with amino acids such as proline, methionine and valine, and organic acids including ascorbic, malic and citric acid (Hegazi, El-Shamy, Fahmy, & Farag, 2021). Since several studies have shown pomegranate benefit in protecting cells from damage and reducing inflammation or the effects of aging (Maphetu, Unuofin, Masuku, Olisah, & Lebelo, 2022), different pomegranate-based formulations have been proposed on the market as effective nutraceutical products to prevent health disease. Recently, Gubitosa et al. (Gubitosa et al., 2018; Gubitosa et al., 2020) presented a novel use for PJ, obtained from wasted fruits, as a reducing agent for Au metal, forming nanostructures with dermatological and cosmetic applications.

Gold nanoparticles have been prepared for years by reductive methods involving aqueous solution of chloroauric acid ($HAuCl_4$) and hazardous reducing and stabilizing agents, namely carbon disulfide or hydrogen peroxide (Daniel & Astruc, 2004; Panda & Chattopadhyay, 2007). To overcome issues related to consumption of large amount of

* Corresponding author.
E-mail address: maria.acquavia@unibas.it (M.A. Acquavia).

https://doi.org/10.1016/j.foodchem.2025.143427
Received 2 October 2024; Received in revised form 12 February 2025; Accepted 13 February 2025
Available online 15 February 2025
0308-8146/© 2025 The Authors. Published by Elsevier Ltd. This is an open access article under the CC BY-NC-ND license (http://creativecommons.org/licenses/by-nc-nd/4.0/).

energy, use of complex equipment and synthesis conditions of chemical and physical methods, the biosynthesis of Au nanoparticles (AuNPs) starting from plant extract is currently proposed as a cost-effective and environmentally friendly alternative, since it is a green chemistry approach that connects nanotechnology with plants (Parveen, Banse, & Ledwani, 2016). Plant extracts are rich in metabolites which could serve as reducing agents of metal ions, thus replacing chemical agents. This is the case of proteins and polyphenols. Accordingly, if temperature and concentration conditions are suitable, green synthesized metal nanoparticles could be produced even with higher quality compared to those obtained by chemical methods (Ying et al., 2022). Furthermore, with respect to the traditional methods, the use of additional capping agents is avoided. Indeed, the molecules from natural origin generally act also as stabilizing agents. These adopted green procedures can be considered non-toxic, pollution-free, environmentally friendly, economical, more sustainable and easily scalable (Ying et al., 2022). In the AuNPs synthesis proposed by Gubitosa et al. (Gubitosa et al., 2018; Gubitosa et al., 2020), the yield was assessed in different reaction volumes with the perspective of scaling up the production at industrial level. In detail, 1 mg/mL of AuNPs was scaled to 1 L as successfully observed, in agreement with the overarching objective of Horizon Europe to bridge the deep gap that exists between academic nanotechnology research and markets. The preliminary costs were evaluated as $\approx$ 0.6 € per Kg (Gubitosa et al., 2020), offering many advantages with respect to the conventional chemical techniques for synthesizing AuNPs (Ying et al., 2022). It is worth mentioning that, for this work, to further reduce the environmental impact, agri-food wastes were used as a resource, and natural sources of bioactive molecules, proposing their recovering according to Circular Economy principles. Not surprisingly, the recovery of agri-food wastes and by-products with the aim to valorize them has a huge interest (Gubitosa et al., 2023; Gubitosa et al., 2023).

PJ represents a well-founded substitute of conventional reducing agents for AuNPs synthesis due to its high content of phenols and flavonoids. Although roles and reaction mechanisms by which PJ phenolic compounds and flavonoids get involved in metal NPs production is still not clearly elucidated, available studies suggested that hydroxyl groups could act as reducing agent for Au^{3+}. The Au(0) produced through this method can collide with adjacent Au(0) atoms, leading to the formation of Au nanoparticles decorated with bioactive molecules. Specifically, these nanoparticles are stabilized by benzoquinone derivatives and polyphenolic compounds generated simultaneously, which create an organic layer surrounding the Au core (Dash & Bag, 2014). Other studies suggested that carboxylic acid could be adsorbed on the Au surface through their carboxylate group which directly forms a bond with the metal (Pala & Toklucu, 2011).

These AuNPs are widely used for medical purposes, since they can adsorb a variety of biomolecules due to their high surface compatibility (Lee et al., 2020). As a matter of fact, AuNPs are used as carriers of anticancer agents (Kumari & Meena, 2020). Moreover, an interest in their light absorption ability, as well as their low toxicity, make AuNPs obtained by means of plant extracts, an advantageous system for potential application in the food packaging industry. Indeed, thanks to the ability of NPs to move into the foodstuff, the development of foodborne pathogens can be avoided, thus extending food shelf life if store in active packaging (Paidari & Ibrahim, 2021; Zhou, Kong, Kundu, Cirillo, & Liang, 2012). So, all these advantages could be considered positive for scaling up the synthesis of nanoparticles at industrial level, offering high earning.

Alongside with their several applications, to date an emerging delight is placed on the characterization of key bioactive compounds participating in the phytosynthesis of Au nanoparticles, in order to control their tunable characteristics (Ahmad et al., 2019). The identification of phytochemicals involved in metal reduction NPs stabilization is challenging due to the complex nature of plant constituents. To date, various spectroscopic techniques have been applied in order to study NPs' composition as well as the composition of the organic layer. UV–Vis does not allow to confirm the attachment of biomolecules to the surface of the synthesized NPs but it grants structural information, i.e. size and shape. On the other hand, with Fourier-transform infrared spectroscopy technique and transmission electron microscopy (TEM), micrographs of phenolic acids or characteristic absorbance peaks for phenolic acids attached to the surfaces of metal NPs could be detected, respectively (Amini & Akbari, 2019). Mass spectrometry (MS) is emerging as a powerful technique for a holistic characterization of NPs, providing elemental and molecular information on structure and chemical state. Moreover, it's highly versatile as it can be coupled with different separation techniques and different ways of sample introduction (Onzo et al., 2020; Pascale et al., 2021). For instance, inductively coupled plasma mass spectroscopy (ICP-MS) allows to provide information on the size distribution, concentration, and elemental composition because of the high-temperature inductively coupled plasma source combined with a mass spectrometer. In this case, a thorough investigation of the sample matrix and its impact on the method's performance characteristics is essential for the accurate determination of NP suspensions (Allabashi, Stach, De La Escosura-Muñiz, Liste-Calleja, & Merkoçi, 2009). So far, combining a powerful chromatographic technique is regarded as a reliable method for separation and real-time assessment of size distributions in nanoparticle mixtures. Size-exclusion chromatography (SEC) is the most commonly used method for this purpose due to its low running costs, quick operation, and reliability, making it a preferred choice for standardizing nanomaterials in solution. SEC-ICP-MS, in particular, has been successfully employed for elemental analysis of gold nanoparticles (Weinberg, Galyean, & Leopold, 2011). Additionally, other chromatographic methods, such as reverse phase chromatography with C18 columns, have been coupled with ICP-MS. For example, gold colloids (5–20 nm) have been successfully characterized and separated by size using a C18 column connected online to ICP-MS, with retention time increasing as AuNP size decreased (Helfrich, Brüchert, & Bettmer, 2006). Unfortunately, the chromatographic techniques have significant limitations when it comes to fractionating nanoparticles with small diameters. For example, liquid chromatography (LC) is plagued by non-specific surface adsorption in the stationary phase and has a restricted size separation range (Helfrich & Bettmer, 2011). These issues hinder the use of SEC or LC for accurately sizing primary nanoparticles and their bioconjugates obtained by plant-extract mediated synthesis.

Anyhow, if preceded by a preliminary washing step in which the phytochemicals are detached from NPs, it is still possible to have insights on the nature of the surrounding organic layer of NPs. For example, Pradeep et al. (Pradeep, Kruszka, Kachlicki, Mondal, & Franklin, 2022) recently evaluated the composition of the organic layer covering AgNPs, establishing the roles of the phytochemicals from *H. perforatum* extract involved in the Ag^{3+} reduction.

Besides, matrix-assisted laser desorption/ionization mass spectrometric analyses (MALDI-MS) can provide other crucial information by correlating entire clusters and aggregates with the actual chemical composition, even in complex nanoparticle-based bioconjugates. MALDI-MS investigations have shown strong capability in characterizing a wide range of AuNPs (with cores containing between 16 and 144 gold atoms), providing sufficient resolution to distinguish between Au_{38} and Au_{40} clusters (Chen, Yu, & Tseng, 2014; Onzo et al., 2021).

In this work, combined analytical methods were used to investigate the role of pomegranate juice in the eco-friendly synthesis of gold nanoparticles. For the first time, an untargeted high-resolution MALDI (−) FT-ICR MS analysis was performed to identify the main metabolite classes involved in AuNPs synthesis. Van Krevelen diagrams were used to illustrate the impact of H/C and O/C ratios of pomegranate metabolites on the synthesis of gold nanoparticles. Moreover, a method based on liquid chromatography coupled to tandem mass spectrometry performed in data-dependent scan was applied to investigate the identity of PJ phytochemicals participating in both synthesis and Au nanoparticles stabilization. Even though the preparation of AuNPs has been previously reported (Gubitosa et al., 2018), here for the first time the combined use

of MALDI FT-ICR MS and LC-ESI-MS/MS can offer a powerful, complementary approach for identifying and characterizing PJ compounds involved in AuNPs green synthesis. MALDI FT-ICR MS provides high-resolution and mass accuracy measurement capable of detecting a broad range of metabolites. On the other hand, LC-MS/MS is particularly effective for identifying low-abundance metabolites, such as specific polyphenols or glycosylated compounds, that might play a crucial role in the synthesis process, also providing kind of quantitative data which can be related to the major or minor role in AuNPs synthesis.

2. Materials and methods

2.1. Chemicals

Gallic acid (97 %), 9-aminoacridine (9-AA, ≥99.5 %), Folin and Ciocalteau phenol reagent and tetrachloroauric acid ($HAuCl_4$) were obtained from Sigma Aldrich (Milan, Italy). The solvents used for LC separation and MS detection, i.e. LC-MS grade methanol (MeOH) and acetonitrile (ACN), were purchased from Sigma-Aldrich (Milano, Italy). Sodium carbonate, ethylacetate, ethanol, and acetone were purchased by Sigma-Aldrich (Milano, Italy). Deionized water used for the analysis was produced through a Water Purification device from Millipore (Bedford, MA, USA).

2.2. Sample preparation

A mixture of wasted Pomegranate fruits, belonging to "Wonderful one" and "Ako" cultivars, was recovered from a local greengrocer located in Bari (south of Italy) and immediately transported to the University of Bari (Dipartimento di Chimica, Via Orabona, 4, Bari, Italy) for juice extraction. Fruits with a uniform shape and consistency were selected. Before extraction, pomegranate fruits were washed with tap water and divided in two halves. Then, the two halves were subjected to manual extraction by using a commercial glass squeezer, according to common protocols for pomegranate juice extraction (Montefusco et al., 2021). As pomegranates were squeezed using commercial glass squeezers, only the arils and seeds actually underwent squeezing in order to recover the corresponding juice. The exocarp and the mesocarp remained almost intact. From this point of view, the edible part of the fruits that was used for the production of juice was always the same, thus ensuring the reproducibility of AuNPs production. The obtained juice was centrifuged for 30 min at 6000 rpm (by using a Thermo Scientific Heraemus Multifuge X3R Centrifuge) for removing the solid residue constituted by peel and seeds and any fragments that may have passed into the liquid. For synthesizing AuNPs, 1.5 mL of a $HAuCl_4$ stock solution 1.0×10^{-3} mol/L, 2 mL of deionized water, and 500 μL of the extracted *Punica Granatum* juice were mixed. Then, the mixture was continuously and moderately stirred (120 rpm stirring speed, Arex, Velp Scientifica) for 4 h at room temperature. The obtained colloidal dispersion (total volume 4 mL) was centrifuged twice for purifying the AuNPs-PJ sample. The wasted supernatant was thus replaced with the same amount of fresh deionized water (4 mL). A final concentration of 2.0×10^{-11} M, that corresponded approximately to 8.5×10^{8} NPs/μL as detailed in (Gubitosa et al., 2018) was inferred. In order to remove PJ excess and unreacted $HAuCl_4$, AuNPs samples were washed with fresh water and centrifuged (7000 rpm, for 10 min). AuNPs pellets and supernatant containing the postreaction residues (PR) were collected separately. For the MALDI FT ICR-MS analyses, PJ, PR and AuNPs samples were mixed with 9-AA (methanolic solution at 15 mg/mL) in a 1:1 ratio and analyzed without any further pre-treatment.

For LC-MS/MS analysis, PJ and the post-reaction residue (PR) were diluted (1:1) in H_2O acidified with formic acid (0.1 %), while AuNPs pellets were dried by lyophilization and washed for the remotion of phytochemicals constituting the organic layer. Compounds adsorbed on the surface of AuNPs were washed serially with LC-MS grade solvents (water, methanol, ethanol, acetone and ethyl acetate), according to a protocol described elsewhere (Pradeep et al., 2022). Briefly, 1 mL of the respective solvent was added to the dried NPs pellets, vortexed for 5 min and sonicated for 15 min at room temperature with a Sonorex Super RK 100/H sonicator. After mixture centrifugation at 20 °C for 30 min, the supernatant was removed. Therefore, the NPs were washed with the next solvent and the supernatant was collected in the same way. At the end of the process, all fractions were reunited in order to pool and characterize the whole pattern of phytochemicals adsorbed on AuNPs surface in a single step. Then, they were subjected to solvent evaporation (Laborota 4000 efficient, Heidolph, Schwabach, Germany). Before injection into the LC-MS/MS analysis, the dried residue was redissolved in 1 mL of H_2O acidified with formic acid (0.1 %) and filtered with 0.2 μm PTFE membrane (Whatman, Maidstone, UK).

2.3. MALDI (−) FT-ICR MS Analysis

A solariX XR 7 T FT ICR-MS equipped with a MALDI ion source (Bruker Daltonik GmbH, Bremen, Germany) was used to acquire high-resolution mass spectra with negative ion mode ionization, in a mass range of 100–2000 *m/z*. Accumulation time was set at 0.1 s, while a 16 M-words time-domain signal was used. The number of scans was set to 50, while laser power and laser shots were set at 32 % and 28, respectively. The mass spectrometer was externally calibrated with a methanolic solution of NaTFA before the analysis in the range 100–2.000 *m/z*. NaTFA is a salt that dissociates in solution to produce sodium ions (Na^+) and clusters. Its use as calibrating solution includes some advantages, i.e. the generation of singly charged ions in both positive and negative ionization modes in low mass range (100–3500 *m/z*), the formation of evenly spaced peaks with similar intensity across the entire mass range, with the most abundant isotope in each mass cluster being the lowest mass peak (monoisotopic mass) which is free from variation in natural isotope distribution. Moreover, it is commercially available. The reached accuracy was calculated in parts per million (ppm) as the difference between the accurate and the exact mass divided for the exact mass, i.e. $((m_a\text{-}m_e)/m_e)\cdot 10^6$, and was lower than 2 ppm (Brenton & Godfrey, 2010; Moini, Jones, Rogers, & Jiang, 1998). Savitzky-Golay algorithm was used for the smoothing of the mass spectra. For peak lists export, a relative intensity threshold of 1.0 % was set. This threshold helped to reduce noise while retaining the most significant peaks for analysis. For PJ and AuNPs samples, as the most intense peaks had intensities (cps) of around 1.5×10^8 and 2×10^9, respectively, a value of 1.0 % allowed to obtain a good balance for ensuring both sensitivity (retaining relevant low-abundance ions) and specificity (reducing noise). From the exported peak lists, possible elemental formulas were calculated for each *m/z* signal. Atoms number limitations, i.e. $C \leq 100$, $H \leq 200$, $O \leq 80$, $N \leq 10$, $S \leq 1$ and $P \leq 1$ (Pascale et al., 2018), restrictions on atoms to carbon number ratios, i.e. $0.2 \leq H/C \leq 3.1$, $O/C \leq 2$, $N/C \leq 1.3$, $S/C \leq 0.8$ and $P/C \leq 0.3$, RDBE >0, nitrogen rule and isotopic pattern filtering were applied to obtain unequivocal formulas for each *m/z* signal. For HRMS data processing Data Analysis was used.

2.4. LC-MS/MS analysis

To profile the compounds occurring in PJ and involved in AuNPs synthesis and stabilization, LC-MS/MS untargeted analyses were conducted on PJ, AuNPs post reaction residues (PR) and solvent-washed AuNPs, using an HPLC system coupled to a LTQ Orbitrap XL mass spectrometer (Thermo Scientific, Bremen, Germany). Samples were filtered through 0.2 μm PTFE membrane before LC-MS/MS analysis. Analytes were chromatographically separated on a Luna C18 (2) (150 × 4.6 mm i.d., 3.0 μm, 100 Å, Phenomenex) column. The mobile phase consisted of solvent A (water +0.1 % formic acid) and solvent B (acetonitrile). The elution gradient was conducted at a constant flow rate of 0.200 mL/min as follows: 0 min, 95 % A; 3 min, 87 % A; 20 min, 50 % A; 35 min, 5 % A; 40 min, 5 % A; initial conditions until 45 min as a re-equilibration step. The injection volume was 25 μL. Negative ion

mode was used for ESI ionization. ESI source parameters were set as follows: tube lens voltage 630 V; capillary temperature 300 °C; spray voltage 2500 V; sheath and auxiliary gas flow (N_2), 50 and 15 a.u. (arbitrary units). *m/z* 200–1600 was used as full range for MS spectra acquisition. Data-dependent scan experiments were employed for MS/MS experiments, fragmenting up to 3 most intense signals in 1 s with an isolation window of ±2.0 *m/z*, at a collision energy of 25 % arbitrary units corresponding to 8.8 eV, and an activation time of 50 ms. The resolution of MS1 and MS2 were set as 60,000. All samples were analyzed in triplicates.

2.5. Determination of the Total phenolic content

The quantitative determination of the total phenolic content (TPC) in pomegranate juice, PJ-Au nanoparticles wash residue and post-reaction residue was conducted according to a modified UV–Vis Folin-Ciocalteu spectrophotometric method (Vernon Singleton Rudolf Orthofer, 1999). Briefly, 60 μL of each sample were mixed with 250 μL of H_2O and 60 μL of Folin and Ciocalteau phenol reagent in microcuvettes. Then, 8 min of equilibrium time were waited and 625 μL of Na_2CO_3 (7 %) and 500 μL of H_2O were added to the samples. Microcuvettes were incubated for 1.5 h

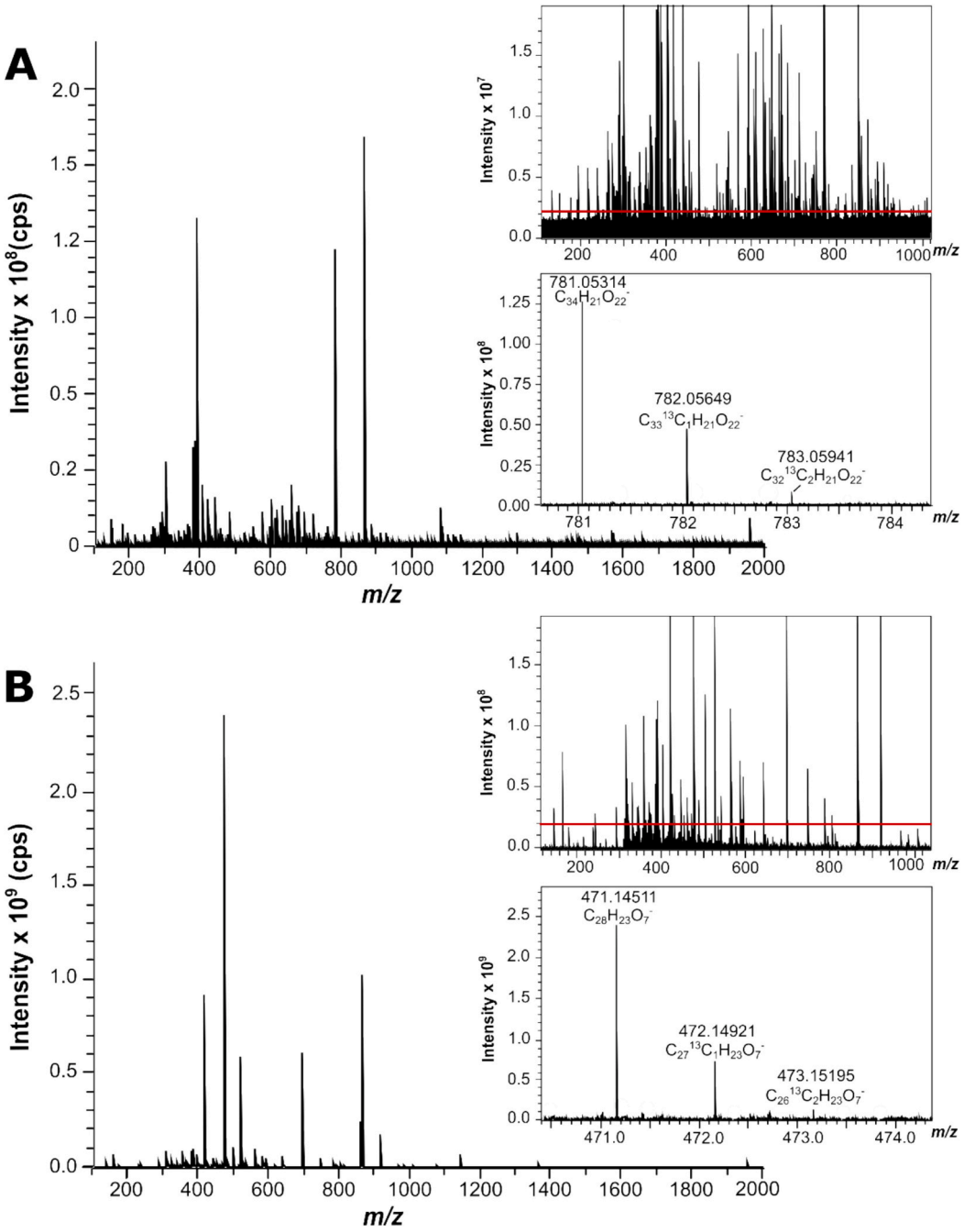


Fig. 1. A, MALDI (−) FT-ICR mass spectrum of pomegranate juice. The insets show a zoom of the signals in the range 100–1000 *m/z* with a red horizontal line highlighting the intensity threshold set for peak list exporting (top) and the isotopic pattern of the ion at *m/z* 781.05314 ($C_{34}H_{21}O_{22}^-$, 1.59 ppm) (level 3 annotation, Salek, Steinbeck, Viant, Goodacre, & Dunn, 2013) (bottom). **B,** MALDI (−) FT-ICR mass spectrum of AuNPs sample. The insets show a zoom of the signals in the range 100–1000 *m/z* with a red horizontal line highlighting the intensity threshold set for peak list exporting (top) and the isotopic pattern of the ion at *m/z* 471.14511 ($C_{28}H_{23}O_7^-$, 0.38 ppm) (level 3 annotation, Salek, Steinbeck, Viant, Goodacre & Dunn, 2013) (bottom). (For interpretation of the references to colour in this figure legend, the reader is referred to the web version of this article.)

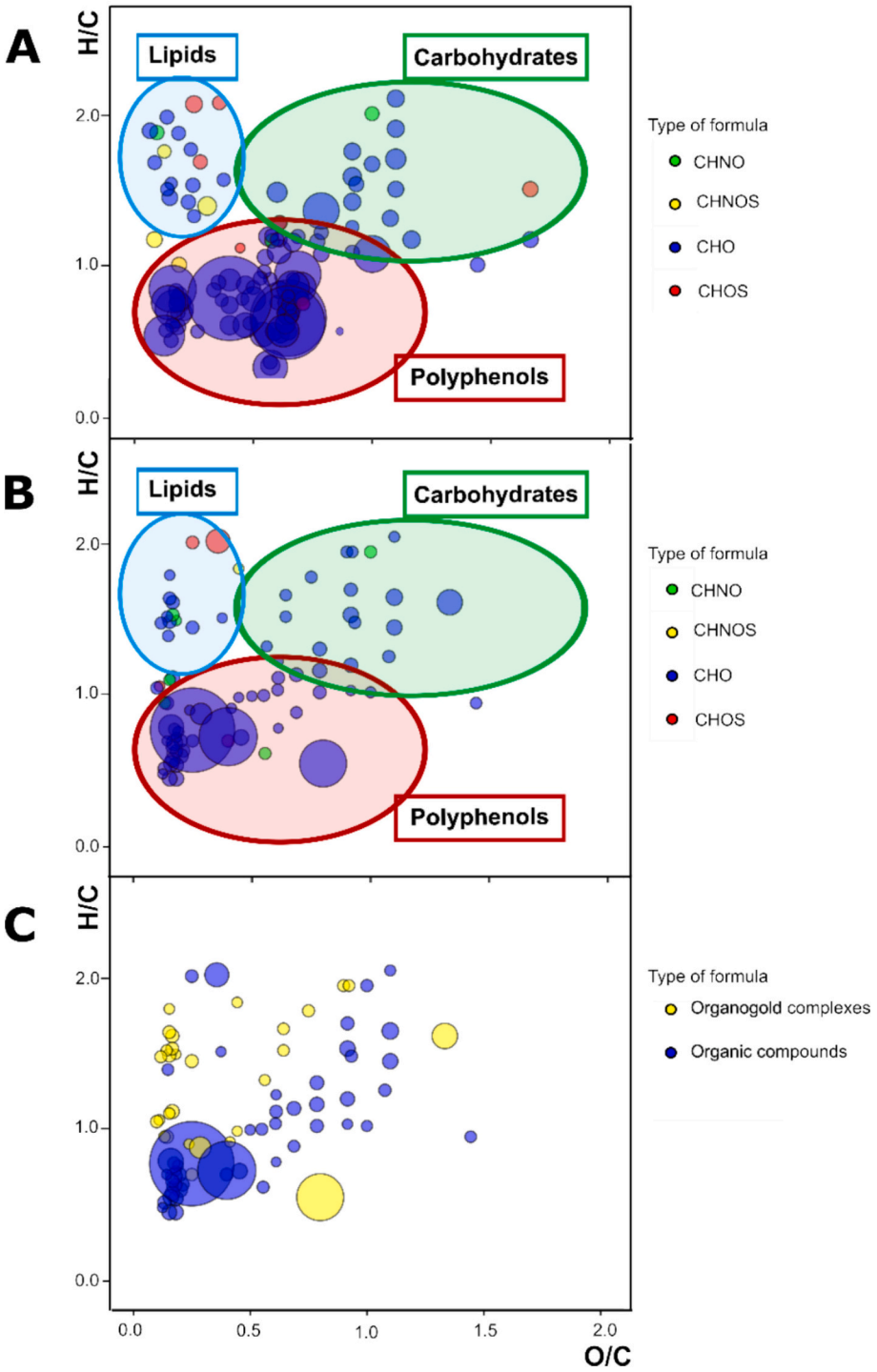


Fig. 2. A, Van Krevelen diagram constructed by using HRMS data of a sample of pomegranate juice (PJ). Different colors were used to differentiate the types of formulae, i.e. green for CHNO, yellow for CHNOS, blue for CHO and red for CHOS formulae. **B,** Van Krevelen diagram of Au nanoparticles (AuNPs) synthesized with pomegranate juice. Different colors were used to differentiate the types of formulae, i.e. green for CHNO, yellow for CHNOS, blue for CHO, and red for CHOS formulae. **C,** Van Krevelen diagram of Au nanoparticles (AuNPs) synthesized with pomegranate juice. Blue and yellow points were used to distinguish organic compounds and organogold complexes, respectively. (For interpretation of the references to colour in this figure legend, the reader is referred to the web version of this article.)

at room temperature after that the absorbance was read at 643 nm using a Cary 1E UV–Visible Spectrophotometer. TPC was calculated using a standard curve of gallic acid (50–1000 μg/mL). All measurements were taken in triplicates.

3. Results and discussion

3.1. MALDI (−) FT-ICR MS Analysis

Matrix-Assisted Laser Desorption Ionization, even thought is a soft ionization technique primarily used in mass spectrometry for the analysis of large biomolecules, polymers, and other complex molecules, when applied to the characterization of metal nanoparticles, offers several advantages. It minimizes NPs fragmentation, thus preserving their core structure during ionization. Organic molecules or ligands that stabilize NPs are less likely to be fragmented as well, thus allowing for better analysis of their surface chemistry. As MALDI typically requires minimal sample preparation, the analysis process is simplified and the potential contamination or alteration of the samples is reduced. Moreover, the combination of MALDI with MS is a powerful tool for the characterization of nanoparticles, especially when it comes to analyzing their surface chemistry, composition, and interactions with other molecules, all while maintaining the integrity of the metallic core (Onzo et al., 2021). In this work, MALDI (−) has been used with Fourier transform ion cyclotron resonance mass spectrometry (FT-ICR-MS) to uncover PJ metabolites participating in AuNPs synthesis. FT-ICR-MS is a highly advanced mass spectrometry technique known for its exceptional resolving power, accuracy, and sensitivity. As it offers very high mass accuracy, here it allowed the exact determination of molecular formulas for both the analyzed complex mixtures, i.e. PJ and AuNPs samples (Onzo et al., 2022). The mass spectra obtained for the two samples are reported in Fig. 1A-B.

A huge number of signals was observed in the MALDI FT-ICR MS spectrum of PJ. A zoom in the range 100–1000 *m/z* showed the details of the spectrum, reflecting the complex composition of the juice, including various metabolites, namely sugars, organic acids, polyphenols, vitamins, and possibly small proteins or peptides. Hundreds of *m/z* signals across a broad mass range could be observed, from small molecules (like amino acids and organic acids) to larger polyphenols or glycosides. As pomegranate juice is rich in polyphenols, signals in the *m/z* range of 200–1000 were mainly noticed. Indeed, this is the common *m/z* range of compounds belonging to the class of flavonoids, phenolic acids, stilbenes, tannins, anthocyanins and their oligomeric derivatives. Accurate mass assignments were carried out using KMD analysis, a widely adopted method for interpreting complex mass spectra, and 14.0151 was used as reference mass (CH_2), as it is commonly used also for metabolomic studies (Ventura et al., 2024). This approach enabled the identification of homologous series and the determination of molecular formulae at high *m/z* ratios (Qian, Rodgers, Hendrickson, Hughey, & Marshall, 2002). Overall, 118 formulae were assigned for PJ (Table S1, Supplementary Information). A level 3 annotation was used to define putatively characterized compounds (Salek et al., 2013). To navigate and interpret the assigned molecular formulae, data were processed for constructing van Krevelen diagrams (VK). A van Krevelen diagram plots the hydrogen-to-carbon (H/C) ratio against the oxygen-to-carbon (O/C) ratio of molecules. The van Krevelen diagram of PJ is shown in Fig. 2A. As expected, several formulae lay in the carbohydrates ($1.53 < H/C < 2.20$ and $0.5 < O/C < 1.23$) and polyphenols area ($0.70 < H/C < 1.34$and $0.16 < O/C < 0.84$) (Laszakovits & MacKay, 2022; Spano et al., 2021). Pomegranate juice is rich in polyphenolic compounds such as ellagic acid and punicalagins. These compounds typically exhibit lower H/C ratios and moderate O/C ratios due to the presence of multiple aromatic rings and hydroxyl groups. For instance, ellagic acid which is an hydrolizable tannin occurring in the analyzed PJ, as confirmed by LC-MS/MS (see through the text), has an H/C and an O/C ratio of 0.4 and 0.6, respectively, and showed here a signal at *m/z* 300.99805 ($C_{14}H_5O_8^-$, 0.52 ppm). Other interesting signals in the polyphenol area corresponded to ions at *m/z* 285.03992 ($C_{15}H_9O_6^-$, 1.96 ppm), *m/z* 301.03478 ($C_{15}H_9O_7^-$, 1.66 ppm), *m/z* 447.05650 ($C_{20}H_{15}O_{12}^-$, 1.56 ppm) and *m/z* 683.18298 ($C_{30}H_{35}O_{18}^-$, 1.74 ppm), putatively assigned to quercetin, kaempferol, kaempferol hexoside and caffeic acid hexoside dimer. Such an assignment was then confirmed by LC-MS/MS data. On other hand, sugars, both monosaccharides or disaccharides such as sucrose, have higher H/C ratios and moderate to high O/C ratios, reflecting their carbohydrate nature. For sucrose, H/C and O/C values are 1.8 and 0.9, respectively. Here, sucrose was putatively identified by its signal at *m/z* 341.10820 ($C_{12}H_{21}O_{11}^-$, 1.06 ppm) and confirmed by LC-MS/MS. Organic acids such as citric acid are also represented with distinct O/C ratios. For example, for citric acid putatively corresponding to ion at *m/z* 191.01875 ($C_6H_7O_7^-$, 0.63 ppm) and confirmed by LC-MS/MS, H/C and O/C values are both 1.2.

It is interesting to notice that the size of the points in the van Krevelen plots is related to a different intensity of the *m/z* signals corresponding to each assigned formula. For PJ sample, the largest points resided in the polyphenol area as the MALDI FT-ICR MS spectrum was dominated by peaks at *m/z* 391.02999 ($C_{17}H_{11}O_{11}^-$, 1.04 ppm) and *m/z* 781.05314 ($C_{34}H_{21}O_{22}^-$, 1.59 ppm), putatively corresponding to citric acid derivative and punicalin, respectively. The observed isotopic patterns supported the elemental formulae assignments that were then confirmed by LC-MS/MS. As example, the isotopic pattern of ion at *m/z* 781.05314 is reported in Fig. 1A**, inset**. A reduced number of formulae standing in the lipids area ($1.34 < H/C < 2.18$ and $0.01 < O/C < 0.35$) was noted in the van Kreleven diagram of PJ. It should be pointed out that the primary source of fatty acids in pomegranate juice is the seeds, that also represent the edible part for PJ production alongside with arils. The oil extracted from pomegranate seeds is rich in fatty acids, and when juiced, some of these fatty acids can be transferred into the juice. Pomegranate oil, which is derived from the seeds, is known for its high content of punicic acid (a conjugated linoleic acid) and other fatty acids (Parashar, 2010). Considering the elemental composition, most of the detected formulae belonged to the types CHO (Fig. 2A). By analyzing the PR with MALDI (−)-FT ICR MS, a molecular fingerprint similar to that obtained for pomegranate juice (**Fig. S1**) was obtained, thus suggesting that compounds present within it were not fully used and depleted during AuNPs green synthesis.

On the other hand, a lower number of *m/z* signals compared to PJ was obtained in the MALDI (−) FT-ICR MS spectra of AuNPs sample (Fig. 1B). Intriguing, most of the putative assigned formulae did not include Au atoms as AuNPs can potentially be destroyed during MALDI-FTICR MS analysis. Indeed, the intense laser energy used in MALDI can lead to rapid desorption and ionization. This high-energy environment may break weak interactions (e.g., hydrogen bonds, π-π interactions) that stabilize gold-polyphenol complexes (Nicolardi et al., 2017). Thus, signals related to PJ phytochemicals participating in AuNPs synthesis and stabilization are expected to be present in the mass spectra both in the gold complexed or un-complexed form. In detail, we supposed that the observed intense ions at *m/z* 471.14511 ($C_{28}H_{23}O_7^-$, 0.38 ppm) (Fig. 1B**, inset**) and *m/z* 863.18319 ($C_{45}H_{35}O_{18}^-$, 0.35 ppm) were involved in AuNPs production and resulted from polyphenols detached from AuNPs surface. Anyway, at least 25 chemical formulae containing up to two Au atoms allowed unequivocal proof of attachment of ligands to the nanoparticles surface. For example, a molecular ion generated by MALDI (−)-FT ICR-MS at *m/z* 871.03678 ($C_{22}H_{21}O_{12}Au_2^-$, 1.06 ppm) was found to correspond to $[M + 2Au–H]^-$ ion (level 3 annotation, Salek et al., 2013). It's worth mentioning that some studies available in literature reported the effective use of gold nanoparticles as the reactive matrix for the detection of compounds in trace levels, such as HCN (Pavlov & Attygalle, 2019). The AuNPs produced in this work using PJ as a reducing agent showed UV–Vis adsorption properties with an adsorption band with a maximum at 577 nm (**Fig. S2**). Therefore, it is possible to assume that AuNPs were also used as their own matrix.

The list of assigned elemental formulae was visualized by two-dimensional van Krevelen diagram (Fig. 2B). The identified molecular

compositions were thus organized in the corresponding molecular classes, including lipids, carbohydrates and polyphenols. Remarkably, a reduced number of molecular annotations was detected in the polyphenol area. Such evidence suggested that they were involved in AuNPs synthesis and stabilization. As a matter of fact, polyphenols generally could stabilize gold nanoparticles better than carbohydrates. This difference arises from their chemical nature, which influences their interaction with AuNPs. Polyphenols have multiple hydroxyl groups (–OH) and other electron-rich moieties that can donate electrons, so allowing the reduction of Au^{3+} ions to elemental gold through a redox reaction. Moreover, their aromatic structure can strongly interact with the surface of AuNPs via π-electron interactions and hydrogen bonding. This forms a robust capping layer that stabilizes the nanoparticles and prevents their aggregation (Tandiana, Sicard-Roselli, Van-Oanh, Steinmann, & Clavaguéra, 2022). In fact, most of the organogold complexes lay in the polyphenol region of the van Krevelen plot (Fig. 2C). On the contrary, carbohydrates, also have hydroxyl groups, but their reducing power is generally weaker compared to polyphenols. Also, many carbohydrates lack aromatic structures or significant π-electron interactions, which limits their ability to strongly adhere to AuNP surfaces (Shervani & Yamamoto, 2011).

In order to better elucidate the structure of the polyphenols contributing to the synthesis and stabilization of AuNPs, an LC-MS/MS analysis was conducted.

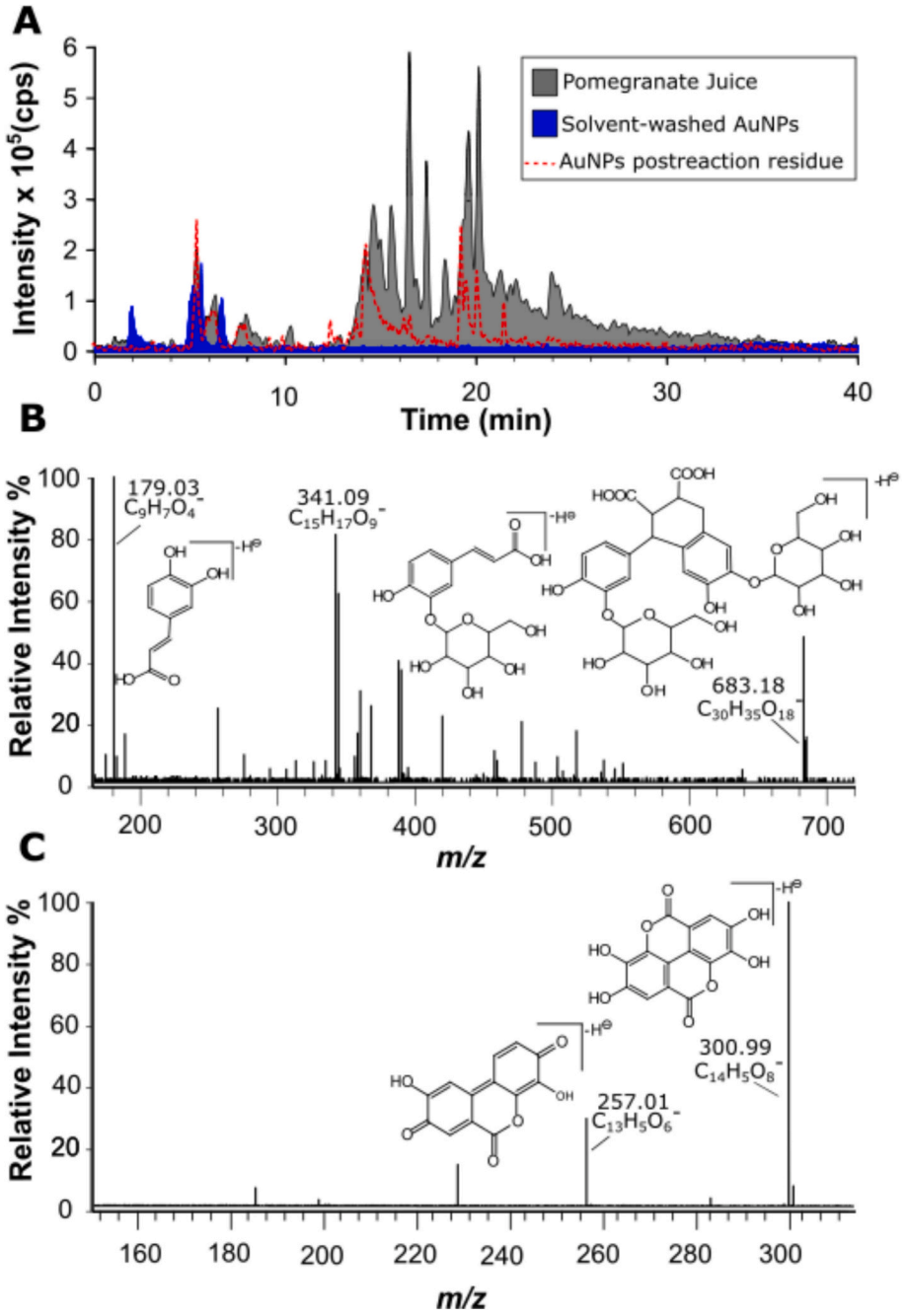


Fig. 3. A, Total Ion Current chromatograms of pomegranate juice, AuNPs postreaction residue and solvent-washed AuNPs, acquired by LC-ESI(−)-MS/MS analysis. **B,** Experimental MS/MS spectrum of negative ion at *m/z* 683.18 identified in PJ as caffeic acid hexoside dimer (level 2 annotation (Salek et al., 2013)), obtained with a collision energy of 25 % arbitrary units corresponding to 8.8 eV. **C,** Experimental MS/MS spectrum of negative ion at *m/z* 300.99 identified in PJ as ellagic acid (level 2 annotation (Salek et al., 2013)), obtained with a collision energy of 25 % arbitrary units corresponding to 8.8 eV.

3.2. LC-MS/MS analysis

In order to identify phenolic compounds present in pomegranate juice that could have been involved in Au nanoparticles phytosynthesis and stabilization, an untargeted LC-ESI-(−)-LTQ-Orbitrap MS/MS-based method was applied. Pomegranate juice composition was the object of numerous studies, mainly focused on restricted groups of phytochemicals, involving complex and long sample pre-treatment steps and time-consuming chromatographic conditions (Mena et al., 2012).

Herein, pomegranate juice was filtered and directly injected into the LC-MS/MS system at the concentration used for AuNPs synthesis without any further pre-treatment protocols. An efficient screening of the complete phenolic profile of PJ was allowed through a chromatographic method based on acetonitrile and water as mobile phase, with the addition of formic acid as additive. Actually, the addition of formic acid to the aqueous phase in LC-MS separations enhances the ionization efficiency, improves peak shape, and increases the overall sensitivity and resolution of the phenolic compounds during analysis of plant extracts (Spáčil, Nováková, & Solich, 2008). Indeed, weak acids could enhance the negative-ion ESI responses due to the strong gas-phase proton affinity of anions, thanks to which the free protons in acidic solution serve merely as counterions, readily reduced during negative-ion ESI (Zengru et al., 2004).

Negative polarity mode was used for compounds detection as $[M-H]^-$ ions, due to the acidic nature of phenols, which readily deprotonate to form stable negative ions, thereby improving their detection and quantification in mass spectrometry. The Total Ion Current (TIC) profile obtained for PJ (Fig. 3A) revealed the presence of 44 major compounds which were putatively identified by accurate mass measurements (root mean square (RMS) error lower than 5 ppm), tandem mass spectrometric experiments, alongside with research in literature data and comparison with mass spectral database available online (http://gnps.ucsd.edu, 2022) according to a level 2 annotation (Salek et al., 2013). Data about the putatively identified compounds, i.e. retention times, *m/z* of the molecular ion detected by using negative ionization and MS/MS fragments, are resumed in Table 1. All the identified compounds were eluted within 30 min of chromatographic run and mostly belonged to the subclasses of hydrolyzable tannins, flavonoids, phenolic acids and carbohydrates. The data obtained were also verified for complementarity with MALDI MS results. LC-MS/MS findings supported putative annotations resulting from MALDI (−) FT ICR MS data.

Hydrolysable tannins (HTs) are an important group of secondary plant metabolites that account for around 92 % of pomegranate antioxidant activity (Passamonti, Vrhovsek, Vanzo, & Mattivi, 2003). HTs include gallic acid derivatives, i.e. gallotannins (GTs), and ellagic acid derivatives, i.e. ellagitannins (ETs). With the exception of galloyl-hexoside (compound **9**, $[M-H]^-$ at *m/z* 331.0654, RMS error 0.77 ppm), all the hydrolysable tannins identified in PJ, i.e. lagerstannin (compound **20**, $[M-H]^-$ at *m/z* 649.0651, RMS error 1.42 ppm), pedunculagin isomer I (compound **27**, $[M-H]^-$ at *m/z* 783.0665, RMS error 0.60 ppm), pedunculagin isomer II (compound **29**, $[M-H]^-$ at *m/z* 783.0667, RMS error 0.48 ppm), punicalagin (compound **30**, $[M-H]^-$ at *m/z* 1083.0579, RMS error 0.11 ppm), punicalin (compound **32**, $[M-H]^-$ at *m/z* 781.0512, RMS error 0.40 ppm), granatin A (compound **33**, $[M-H]^-$ at *m/z* 799.0622, RMS error 0.15 ppm), ellagic acid hexoside (compound **34**, $[M-H]^-$ at *m/z* 463.0502, RMS error 0.50 ppm), corilagin (compound **35**, $[M-H]^-$ at *m/z* 633.0726, RMS error 0.25 ppm) and granatin B (compound **36**, $[M-H]^-$ at *m/z* 951.0725, RMS error 0.43 ppm), belonged to the class of ETs, as confirmed by fragment ion at *m/z* 300.99 ($C_{14}H_5O_8^-$) corresponding to ellagic acid ion (Enomoto, 2021; Fischer et al., 2011).

As flavonoids, mainly kaempferol and quercetin glycosidic derivatives, alongside with catechin (compound **18**, $[M-H]^-$ at *m/z* 289.0718, RMS error 1.76 ppm), epicatechin (compound **1**, $[M-H]^-$ at *m/z* 289.0720, RMS error 2.06 ppm) and its derivative, i.e. epigallocatechin-7-*O*-glucuronide (compound **19**, $[M-H]^-$ at *m/z* 481.0971, RMS error 0.53 ppm) were identified (Abid et al., 2017; Díaz-Mula, Tomás-Barberán, & García-Villalba, 2019; Fischer et al., 2011; Man, Xu, Wang, Liao, & Xu, 2022; Mena et al., 2012). Kaempferol was identified by molecular ion $[M-H]^-$ at *m/z* 285.0393 (RMS error 0.10 ppm), while the presence of the 3,4′,5,7-tetrahydroxyflavone aglycone for kaempferol-hexoside (compound **15**, $[M-H]^-$ at *m/z* 447.0514, RMS error 0.90 ppm) was ascertained by signal at *m/z* 285.04 ($C_{15}H_9O_6^-$) (Ma, Li, Van Den Heuvel, & Claeys, 1997) and supported by level 3 annotation based on MALDI MS data. Moreover, dihydrokaempferol-hexoside was identified (compound **37**, $[M-H]^-$ at *m/z* 449.1072, RMS error 0.64 ppm). On the other hand, for quercetin glycosidic derivatives, i.e. isorhamnetin-hexoside (compound **6**, $[M-H]^-$ at *m/z* 477.1028, RMS error 0.04 ppm), rutin (compound **16**, $[M-H]^-$ at *m/z* 609.1452, RMS error 0.14 ppm), rutin hydrate (compound **17**, $[M + H_2O-H]^-$ at *m/z* 627.1548, RMS error 0.55 ppm), quercetin rhamnoside (compound **22**, [M-H]- at *m/z* 447.0916, RMS error 0.59 ppm), a signal at *m/z* 301.03 ($C_{15}H_9O_7^-$) corresponding to quercetin aglycone was observed (Acquavia et al., 2021; EL-Aguel et al., 2022; Mena et al., 2012). Two myricetin derivatives, i.e. myricetin rhamnopyranoside (compound **10**, $[M-H]^-$ at *m/z* 463.0861, RMS error 0.97 ppm) and myricetin glucopyranoside (compound **24**, $[M-H]^-$ at *m/z* 479.0817, RMS error 0.30 ppm) were identified as well (http://gnps.ucsd.edu, 2022; Man et al., 2022). It is interesting to notice that myricetin glucopyranoside has never been reported before in *Punica granatum*. Moreover, for the subclass of flavonoids, the presence of 2-(3,5-dihydroxy-1,4-dioxo-1,4-dihydronaphthalen-2-yl)-3-methoxy-5-methylbenzoic acid (compound **7**, $[M-H]^-$ at *m/z* 353.0705, RMS error 1.21 ppm), dihydrokaempferol (compound **11**, $[M-H]^-$ at *m/z* 287.0549, RMS error 0.18 ppm), luteolin (compound **14**, $[M-H]^-$ at *m/z* 285.0392, RMS error 0.26 ppm), methyl 2-(9-hydroxy-1-methyl-5,10-dioxo-3,4-dihydro-1H-benzo[*g*]isochromen-3-yl)acetate (compound **40**, $[M-H]^-$ at *m/z* 315.0860, RMS error 0.40 ppm), and isotectorigenin, 7-methyl ether (compound **41**, $[M-H]^-$ at *m/z* 327.0859, RMS error 0.57 ppm) and scutellarioside (compound **42**, $[M-H]^-$ at *m/z* 507.1489, RMS error 0.71 ppm) was confirmed (http://gnps.ucsd.edu, 2022; Man et al., 2022; Van Elswijk, Schobel, Lansky, Irth, & Van Der Greef, 2004). While dihydrokaempferol and luteolin have been previously reported in pomegranate pericarp (http://gnps.ucsd.edu, 2022; Man et al., 2022; Van Elswijk et al., 2004), methyl 2-(9-hydroxy-1-methyl-5,10-dioxo-3,4-dihydro-1H-benzo[*g*]isochromen-3-yl)acetate, isotectorigenin, 7-methyl ether and scutellarioside have been putatively identified in PJ for the first time. In addition to tannins and flavonoids, phenolic acids, like caffeic acid hexoside dimer (compound **5**, $[M-H]^-$ at *m/z* 683.1823, RMS error 0.33 ppm), ferulic acid hexoside (compound **12**, $[M-H]^-$ at *m/z* 355.1025, RMS error 0.18 ppm), vanillic acid hexoside (compound **13**, $[M-H]^-$ at *m/z* 329.0866, RMS error 0.15 ppm), ellagic acid (compound **21**, $[M-H]^-$ at *m/z* 300.9979, RMS error 0.01 ppm), and ellagic acid pentoside (compound **39**, $[M-H]^-$ at *m/z* 433.0397, RMS error 0.47 ppm) were found in PJ (Fischer et al., 2011). Interestingly, caffeic acid hexoside dimer is unprecedented in PJ. One possible way through which caffeic acid hexoside is converted into its dimer involves the conversion of the molecule into a semiquinone radical during a one-electron oxidation, hence followed by a coupling reaction (Arakawa, Yamaguchi, Hotta, Osakai, & Kimoto, 2004). The existence of the dimer in PJ was supported by MS/MS data, as fragment ion at *m/z* 341.09 ($C_{15}H_{17}O_9^-$), corresponding to the monomeric unit of the molecule, was detected. Moreover, a typical ion fragment at *m/z* 179.03 ($C_9H_7O_4^-$) due to the loss of a hexose moiety (−162 Da) was noticed (Fig. 3**.B**). These results confirmed level 3 annotations of ion at *m/z* 683.18298 ($C_{30}H_{35}O_{18}^-$, 1.74 ppm) based on MALDI MS data. As regard to ellagic acid, it is often selected as an intrinsic chemical marker for commercial standardization of pomegranate supplements, to ensure that supplements contain genuine pomegranate fruit extract (Zhang, Wang, Lee, Henning, & Heber, 2009). The diagnostic ion fragment observed into its MS/MS spectra at *m/z* 257.01, was due to the opening of the lactone ring with subsequent loss of CO_2 (Ramirez, Zambrano, Sepúlveda, & Simirgiotis, 2014) (Fig. 3**.C**).

Table 1
Main phenolic compounds identified through a level 2 annotation (Salek et al., 2013) in pomegranate juice (PJ), AuNPs postreaction residue (PR) and solvent-washed AuNPs (SW) by LC-ESI(−)-MS/MS analysis.

Compound N.	RT (min)	Proposed compound	Phenols Subclass	Molecular formula	[M-H]$^-$ (*m/z*)	Resolution	RMS error[a] (ppm)	MS/MS fragments	PJ	PR	SW	References
1	5.5	Epicatechin	Flavonoid	$C_{15}H_{13}O_6^-$	289.0720	64,904	2.06	245.08; 179.03; 151.04; 137.02	+	+	+	(Díaz-Mula et al., 2019; Mena et al., 2012)
2	7.8	Disaccharide	Carbohydrate	$C_{12}H_{23}O_{12}^-$	359.1176	50,704	1.00		+	+	−	(http://gnps.ucsd.edu, 2022)
3	8.0	α-D-Glucopyranoside, α-D-fructofuranosyl	Carbohydrate	$C_{12}H_{23}O_{11}^-$	343.1230	35,004	0.64		+	+	−	(http://gnps.ucsd.edu, 2022)
4	8.1	Sucrose	Carbohydrate	$C_{12}H_{21}O_{11}^-$	341.1076	50,704	0.31	179.06	+	+	+	(http://gnps.ucsd.edu, 2022)
5	8.2	Caffeic acid hexoside dimer	Phenolic acid	$C_{30}H_{35}O_{18}^-$	683.1823	33,604	0.33	179.03; 341.09	+	+	+	(http://gnps.ucsd.edu, 2022
6	8.5	Isorhamnetin-hexoside	Flavonoid	$C_{22}H_{21}O_{12}^-$	477.1028	33,004	0.04	314.04; 301.03	+	−	+	(Man et al., 2022)
7	14.2	2-(3,5-dihydroxy-1,4-dioxo-1,4-dihydronaphthalen-2-yl)-3-methoxy-5-methylbenzoic acid	Flavnonoid	$C_{12}H_{17}O_{12}^-$	353.0705	54,504	1.21	121.09	+	+	−	(http://gnps.ucsd.edu, 2022)
8	14.8	Citric acid	Carboxylic acid	$C_6H_7O_7^-$	191.0192	65,704	1.34	111.01	+	+	−	(Sentandreu, Cerdán-Calero, & Sendra, 2013)
9	15.2	Galloyl - hexoside	Hydrolizable tannin	$C_{13}H_{15}O_{10}^-$	331.0654	35,004	0.77	300.10; 169.01	+	+	−	(Fischer et al., 2011)
10	15.7	Myricetin rhamnopyranoside	Flavonoid	$C_{21}H_{19}O_{12}^-$	463.0861	36,104	0.97	317.25	+	−	−	(Man et al., 2022)
11	15.9	Dihydrokaempferol	Flavonoid	$C_{15}H_{11}O_6^-$	287.0549	64,904	0.18	259.06	+	+	−	(Man et al., 2022)
12	16.1	Ferulic acid hexoside	Phenolic acid	$C_{16}H_{19}O_9^-$	355.1025	50,704	0.18		+	+	−	(Fischer et al., 2011)
13	16.2	Vanillic acid hexoside	Phenolic acid	$C_{14}H_{17}O_9^-$	329.0866	48,704	0.15	191.03; 167.03	+	+	−	(Fischer et al., 2011)
14	16.3	Luteolin	Flavonoid	$C_{15}H_9O_6^-$	285.0392	64,904	0.26	271.05	+	+	−	(Van Elswijk et al., 2004)
15	16.4	Kaempferol hexoside	Flavonoid	$C_{20}H_{15}O_{12}^-$	447.0514	36,104	0.90	285.04; 255.51	+	+	−	(Mena et al., 2012)
16	16.5	Rutin	Flavonoid	$C_{27}H_{29}O_{16}^-$	609.1452	33,604	0.14	301.03; 300.03	+	−	−	(Man et al., 2022)
17	16.6	Rutin hydrate	Flavonoid	$C_{27}H_{31}O_{17}^-$	627.1548	33,004	0.55	301.03	+	+	−	(http://gnps.ucsd.edu, 2022)
18	16.7	Catechin	Flavonoid	$C_{15}H_{13}O_6^-$	289.0718	81,904	1.76	245.08; 203.07; 179.03; 151.03; 125.02; 109.03	+	−	+	(Díaz-Mula et al., 2019; Mena et al., 2012)
19	16.9	Epigallocatechin-7-*O*-glucuronide	Flavonoid	$C_{21}H_{21}O_{13}^-$	481.0971	48,704	0.53	300.99	+	−	+	(Fischer et al., 2011)
20	17.1	Lagerstannin	Hydrolizable Tannin	$C_{27}H_{21}O_{19}^-$	649.0651	33,604	1.42	486.98; 300.99	+	−	−	(Fischer et al., 2011)
21	17.3	Ellagic Acid	Hydrolizable Tannin	$C_{14}H_5O_8^-$	300.9979	64,004	0.01	257.01	+	+	−	(Fischer et al., 2011)
22	17.4	Quercitin rhamnoside	Flavonoid	$C_{21}H_{19}O_{11}^-$	447.0916	54,504	0.59	301.03	+	−	−	(EL-Aguel et al., 2022)
23	17.5	Kaempferol	Flavonoid	$C_{15}H_9O_6^-$	285.0393	64,904	0.10	257.04	+	+	−	(Van Elswijk et al., 2004)
24	17.6	Myricetin glucopyranoside	Flavonoid	$C_{21}H_{19}O_{13}^-$	479.0817	36,104	0.30		+	−	−	(http://gnps.ucsd.edu, 2022)
25	18.0	3,4-methylenedioxycinnamic acid	Carboxylic acid	$C_8H_5O_4^-$	165.0187	65,704	1.26	137.02	+	+	−	(http://gnps.ucsd.edu, 2022)
26	18.2	Citric acid derivative	Carboxylic acid	$C_{17}H_{11}O_{11}^-$	391.0310	35,004	1.62	217.02	+	+	−	(Mena et al., 2012)
27	18.4	Pedunculagin isomer I	Hydrolizable Tannin	$C_{34}H_{23}O_{22}^-$	783.0665	33,004	0.60	765.06;300.99	+	+	−	(Fischer et al., 2011; Sentandreu et al., 2013)
28	19.1	Demethyloleuropein	Terpene Glycoside	$C_{24}H_{29}O_{13}^-$	525.1598	45,904	0.40		+	−	−	(http://gnps.ucsd.edu, 2022)
29	19.4	Pedunculagin isomer II	Hydrolizable Tannin	$C_{34}H_{23}O_{22}^-$	783.0667	37,204	0.48	300.99	+	−	−	(Fischer et al., 2011; Sentandreu et al., 2013)
30	19.5	Punicalagin α	Hydrolizable Tannin	$C_{48}H_{27}O_{30}^-$	1083.0579	30,304	0.11	781.05; 600.99; 300.99	+	+	−	(Fischer et al., 2011)
31	19.6	Quercetin	Flavnonoid	$C_{15}H_9O_7^-$	301.0342	33,604	0.12	257.01	+	+	−	(Van Elswijk et al., 2004)
32	19.7	Punicalin	Hydrolizable Tannin	$C_{34}H_{21}O_{22}^-$	781.0512	37,204	0.40	600.99; 300.99	+	+	−	(Fischer et al., 2011)
33	19.7	Granatin A	Hydrolizable Tannin	$C_{34}H_{23}O_{23}^-$	799.0622	29,704	0.15	300.99	+	+	−	(Fischer et al., 2011)
34	20.1	Ellagic acid hexoside	Hydrolizable Tannin	$C_{20}H_{15}O_{13}^-$	463.0502	36,104	0.50	300.99	+	−	−	(Mena et al., 2012)
35	20.2	Corilagin	Hydrolizable Tannin	$C_{27}H_{21}O_{18}^-$	633.0726	54,504	0.25	463.05; 300.99	+	−	−	(Enomoto, 2021; Fischer et al., 2011)
36	21.4	Granatin B	Hydrolizable Tannin	$C_{41}H_{27}O_{27}^-$	951.0725	40,504	0.43	300.99	+	+	−	(Fischer et al., 2011)

(*continued on next page*)

Table 1 (*continued*)

Compound N.	RT (min)	Proposed compound	Phenols Subclass	Molecular formula	$[M-H]^-$ (*m/z*)	Resolution	RMS error[a] (ppm)	MS/MS fragments	PJ	PR	SW	References
37	21.5	Dihydrokaempferol-hexoside	Flavonoid	$C_{21}H_{21}O_{11}^-$	449.1072	48,704	0.64	287.06; 151.00	+	+	–	(Fischer et al., 2011; Regos, Urbanella, & Treutter, 2009)
38	21.6	Kanokoside A	Oligopeptide	$C_{21}H_{31}O_{12}^-$	475.1798	45,904	1.13	205.07; 101.02	+	–	–	(http://gnps.ucsd.edu, 2022)
39	22.3	Ellagic acid pentoside	Phenolic acid	$C_{19}H_{13}O_{12}^-$	433.0397	54,504	0.47	300.99	+	+	–	(Fischer et al., 2011)
40	22.6	methyl 2-(9-hydroxy-1-methyl-5,10-dioxo-3,4-dihydro-1H-benzo[g]isochromen-3-yl) acetate	Flavonoid	$C_{17}H_{15}O_6^-$	315.0860	35,004	0.45		+	+	–	(http://gnps.ucsd.edu, 2022)
41	22.7	Isotectorigenin, 7-Methyl Ether	Flavonoid	$C_{18}H_{15}O_6^-$	327.0859	50,704	0.57	312.06	+	+	–	(http://gnps.ucsd.edu, 2022)
42	22.8	Scutellarioside	Flavonoid	$C_{24}H_{27}O_{12}^-$	507.1489	45,904	0.71		+	–	–	(http://gnps.ucsd.edu, 2022)
43	23.2	Carminic Acid	Carboxylic acid	$C_{22}H_{19}O_{13}^-$	491.0813	48,704	0.65		+	+	–	(http://gnps.ucsd.edu, 2022)
44	25.0	Phlorhizin	Dihydrochalcone	$C_{21}H_{23}O_{10}^-$	435.1282	54,504	0.38	271.00	+	–	+	(Lijia, Guo, Chen, Baoping, & Zhang, 2014)

[a] Mass accuracy expressed as root-mean-square (RMS) in part per million (ppm) of five ($n = 5$) *m/z* measurements.

As expected, the used method for the chromatographic separation allowed the detection of some carbohydrates in PJ, namely disaccharide (compound **2**, $[M-H]^-$ at *m/z* 359.1176, RMS error 2.00 ppm), α-D-Glucopyranoside, α-D-fructofuranosyl (compound **3**, $[M-H]^-$ at *m/z* 343.1230, RMS error 0.64 ppm) and sucrose (compound **4**, $[M-H]^-$ at *m/z* 341.1076, RMS error 0.31 ppm) (http://gnps.ucsd.edu, 2022), previously assigned by MALDI MS data with a level 3 annotation. All the identified carbohydrates, contributing to PJ's natural sweetness, were eluted in the first 10 min of the chromatographic run.

To uncover the role of the pomegranate juice in AuNPs synthesis, the developed untargeted LC-ESI(−)-LTQ-Orbitrap MS/MS-based method was applied for profiling the phytochemicals occurring in AuNPs post reaction residues (PR). The results revealed that most of the compounds identified in pristine PJ were still present in the supernatant, albeit the area of the corresponding chromatographic signals was reduced. These findings were in accordance with those obtained by MALDI MS analysis, as MALDI (−) FT ICR MS spectra for both PJ and PR showed a similar profile, although less intense *m/z* signals were observed for PR sample. As both samples, i.e. PJ and PR, were diluted 1:1 with H_2O acidified with 0.1 % of formic acid, it could be assumed that the reduction of the area of the chromatographic signals corresponding to each identified molecule was not related to a different dilution factor between the two samples. Therefore, the area of the chromatographic signal corresponding to each identified molecule was used to find out the Au^{3+} reducers and/or the AuNPs stabilizers. In detail, 29 compounds were detected in PR (Table 1). A mean reduction of ~80 % was observed for all the values of the areas, except for epicatechin (compound **1**), sucrose (compound **4**), maltosylsucrose (compound **5**) and 3,4-methylenedioxycinnamic acid (compound **25**). In these cases, reductions of ~30 %, ~62 %, ~9 % and ~ 31 % were observed, respectively. On the other hand, among all the compounds identified in PJ, 15 were completely depleted in PR (Fig. 4). As previously reported in literature data, it's possible to assume that compounds reduced or depleted in PR sample acted as reducing agent for Au^{3+} (Pradeep et al., 2022). Interestingly, all metabolites that were completely absent in postreaction residue, mainly belonged to the subclass of flavonoids. Flavonoids reducing power is due to their polyphenolic structure, which includes multiple hydroxyl groups. The hydroxyl groups can donate hydrogen atoms or electrons to free radicals, stabilizing them and preventing oxidative damage to cells. This ability to act as both hydrogen or electrons donors makes them well known antioxidants and powerful reducing agents (Firuzi, Lacanna, Petrucci, Marrosu, & Saso, 2005). For what concerns tannins, they generally have higher reducing power compared to flavonoids. This is due to the higher number of hydroxyl groups occurring in their structure, which contribute to their strong antioxidant activity and ability to donate electrons or hydrogen atoms to neutralize free radicals. Here, the lower number of hydrolysable tannins involved in Au^{3+} reductions could be due to the lower number of HT available in PJ with respect to flavonoids. For instance, an absence of chromatographic signals related to ellagic acid hexoside (**compound 34**) in PR let to infer that it was involved in AuNPs reduction, confirming level 3 assignment of MALDI FT ICR MS data. In detail, signal at *m/z* 463.05142 ($C_{20}H_{15}O_{13}^-$, 1.53 ppm) in the MALDI MS spectrum of AuNPs was most probably due to ellagic acid hexoside detached from AuNPs surface.

The LC-MS/MS chromatogram of solvent-washed AuNPs allowed to establish putative stabilizing agents of the synthetized nanoparticles. NPs stabilization is crucial for several reasons, particularly in ensuring their functionality, safety, and applicability in various fields. Since they have a high surface area-to-volume ratio, which can lead to a strong tendency to agglomerate or cluster together, stabilization is requested to held a uniform dispersion, ensuring they remain as individual particles with the desired properties (Raveendran, Fu, & Wallen, 2003). A reduced number of compounds compared to PJ and PR was ascertained in solvent-washed AuNPs, i.e. epicatechin (compound **1**), sucrose (compound **4**) and caffeic acid hexoside dimer (compound **5**) (Fig. 4).

It is worth mentioning that epicatechin, sucrose and caffeic acid

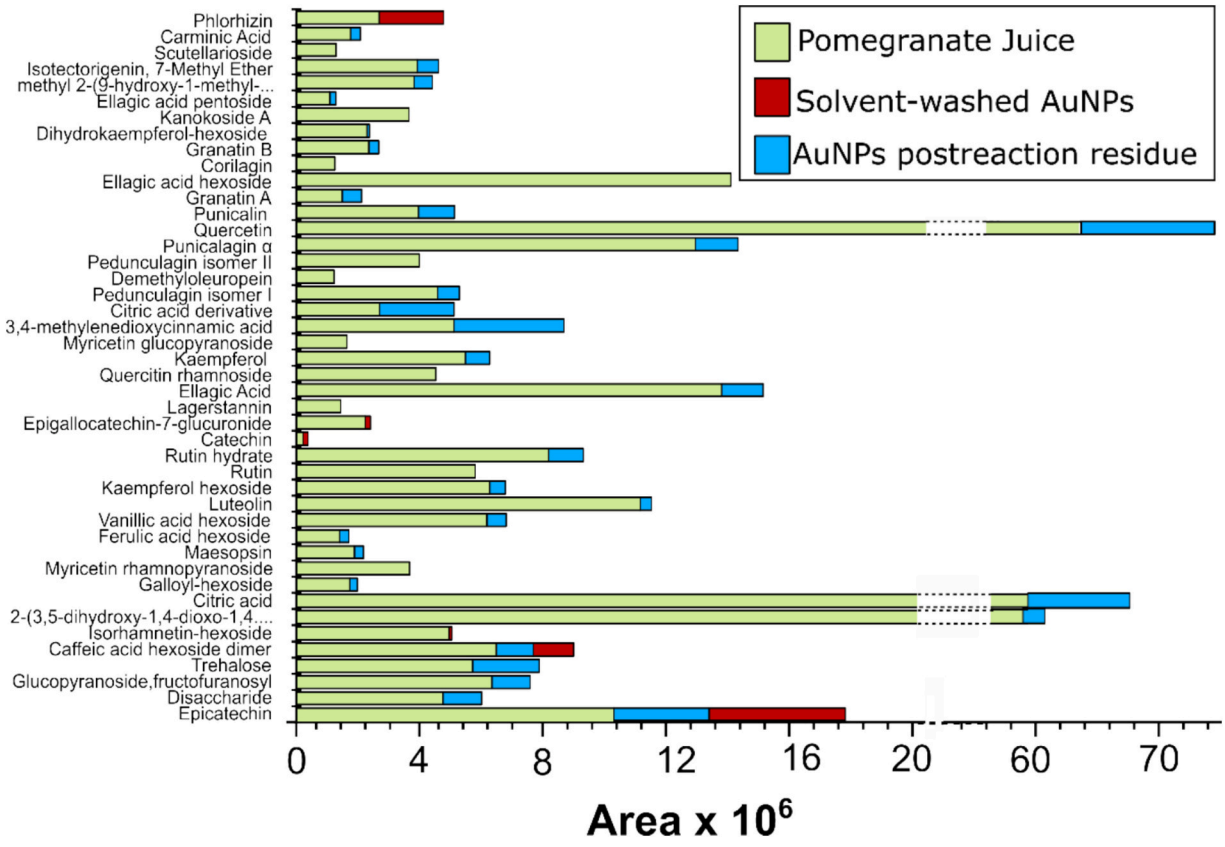


Fig. 4. Area of the chromatographic signals corresponding to the 44 compounds detected in pomegranate juice, AuNPs postreaction residue and solvent-washed AuNPs by LC-ESI(−)-MS/MS analysis, according to a level 2 annotation (Salek et al., 2013).

hexoside dimer are among the compounds identified in postreaction residue undergoing a minor reduction in the area of the corresponding chromatographic signals. Actually, sucrose has a low reducing power which could explain their greater role as capping agents. Indeed, it is a disaccharide made of two glucose molecules linked by an α,α-1,1-glycosidic bond. Since the anomeric carbons are engaged in the glycosidic bond, sucrose lacks a free aldehyde or keto group which can participate in redox reactions typical of reducing sugars.

As regard to epicatechin and caffeic acid derivative, the obtained results confirmed the results obtained by MALDI (−)-FT ICR MS analysis, suggesting that they were mainly involved in AuNPs synthesis and stabilization, presumably binding themself to the surface of metal nanoparticles. The interaction with the phenolic groups can create a protective layer around them, preventing agglomeration and growth. More in detail, the presence of multiple hydroxyl groups in epicatechin and caffeic acid hexoside dimer can lead to both electrostatic and steric stabilization. Electrostatic stabilization may occur when -OH creates a charge around NPs, leading to repulsion between them. On the other hand, steric stabilization takes place as the bulky epicatechin and caffeic acid derivative molecules can physically block NPs from coming too close together (Fig. 5A). In addition, isorhamnetin-hexoside (compound **6**), catechin (compound **18**), epigallocatechin-7-*O*-glucuronide (compound **19**) and phlorhizin (compound **44**) were identified as well in solvent-washed AuNPs. Unlike the ones mentioned before, the latter were not present in the PR sample (Fig. 5B), thus clarifying their unique function in nanoparticles' stabilization. The presence of sugar moieties in the flavonoids structure may have enhanced the overall stabilization due to the increased water solubility through hydrogen bonding and hydrophilic interactions (Saleemi, Alallam, Yong, & Lim, 2022).

The results obtained by the overall LC-MS/MS analysis suggested that pomegranate juice could be used as an excellent vehicle to synthetize AuNPs.

3.3. Determination of Total Polyphenol Content

To quantitatively evaluate the content the role of PJ's bioactive compounds in nanoparticles green synthesis, pomegranate juice, as well as the postreaction residue and the solvent-washed AuNPs, were analyzed in triplicates for their total polyphenol content (TPC) according to a modified Folin-Ciocalteu spectrophotometric method. The mean total polyphenol concentration in PJ was 18.77 ± 0.12 μg/mL of gallic acid equivalents, while for postreaction residue and solvent-washed AuNPs, mean values of 11.15 ± 0.11 and 2.52 ± 0.02 μg/mL of gallic acid equivalents were found, respectively. Hence, for PR a reduction of 50 % was observed relative to the initial content of polyphenolic compounds occurring in PJ, according to previous results available in the literature (Ahmad et al., 2019; Alegria et al., 2018). For instance, Ahmad et al. (Ahmad et al., 2019) found that over 60 min of reaction time, the amount of phenols passed from 48.08 ± 1.98 mg of GAE up to 9.59 ± 0.92 mg of GAE for AuNPs produced using aqueous *Elaeis guineensis* leaves extract. Here, the obtained results confirmed the significant contribution of phenolic compounds, as about half of their total amount found in pomegranate juice was effectively involved in the synthesis and stabilization of AuNPs. On the other hand, such findings perfectly align with the outcomes obtained through LC-MS/MS analyses. The decrease observed in the overall levels of phenolic compounds could be attributed to their involvement as agents responsible for both the reduction and the stabilization processes during nanoparticles formation.

4. Conclusions

In this work, the combined use of MALDI FT-ICR MS and LC-ESI-MS/MS disclosed a powerful, complementary approach for identifying and characterizing PJ's metabolites participating in AuNPs green synthesis. For the first time by providing qualitative data on the metabolites

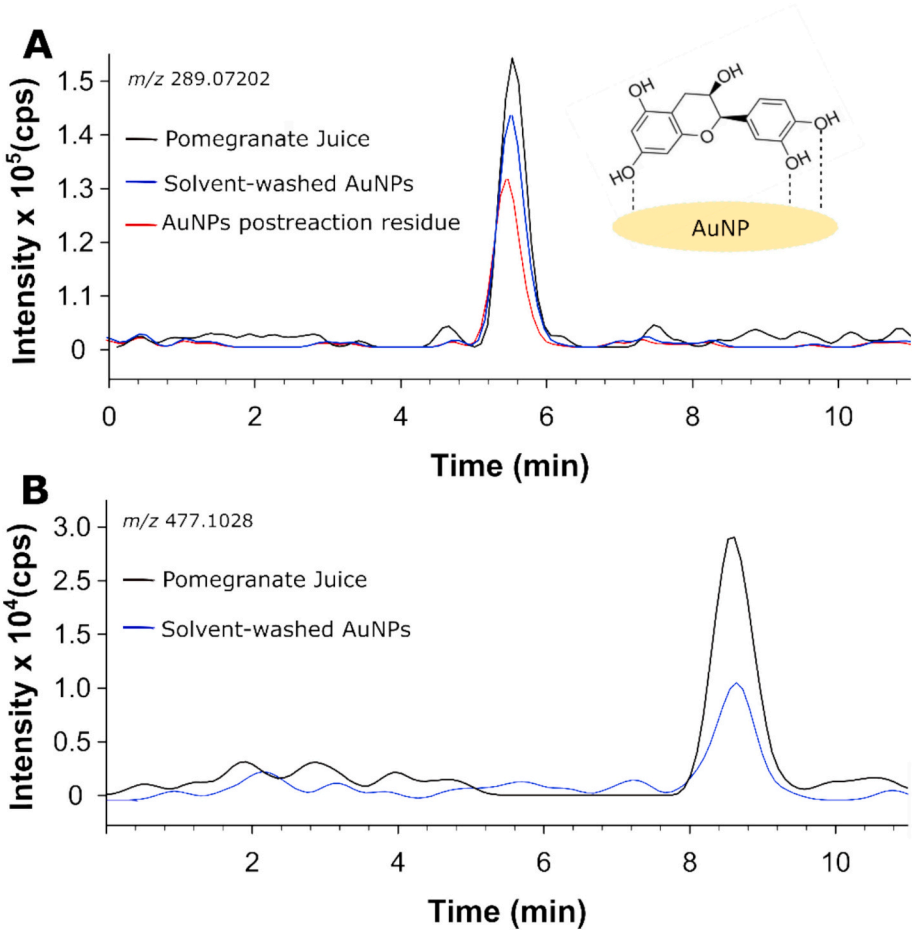


Fig. 5. A, Extracted ion current (XIC) chromatograms by LC-ESI-MS/MS acquired in negative ion mode of epicatechin (compound **1**, *m/z* 289.0720) and **B,** isorhamnetin-hexoside (compound **6**, *m/z* 477.1028) detected in pomegranate juice, solvent-washed AuNPs and/or AuNPs postreaction residue.

involved, this approach improved the understanding of PJ's role in AuNPs synthesis and also advanced the development of eco-friendly and biocompatible nanoparticle synthesis methods, with significant implications in various scientific and industrial applications. MALDI FT-ICR MS and van Krevelen diagrams, used as visualization tool for high-resolution mass spectrometric data, allowed to establish the main classes of compounds involved in the stabilization of the produced gold nanoparticles. The results indicated that polyphenols played a significant role in the synthesis and stabilization of the produced nanoparticles. On the other hand, LC-MS/MS analysis let to separate and elucidate the in-depth structure of phenols acting as reducing and/or capping agents. The outcomes of the chromatographic separation coupled to tandem mass spectrometric detection performed in data-dependent acquisition, suggested that reducing agents mainly belonged to the subclass of flavonoids. The significant contribution of phenolic compounds in the reduction of Au^{3+} into gold atoms achieved through the use of pomegranate juice was quantified by a spectrophotometric assay. The potential of using natural plant extracts like PJ in sustainable nanotechnology, has been highlighted. The deep comprehension of the natural polyphenols' role in AuNPs synthesis opens avenues for sustainable nanoparticle production, offering a cost-effective and environmentally friendly alternative to traditional chemical methods. The provided insights can guide the optimization of large-scale, affordable production methods in industrial applications. This aligns with global sustainability initiatives, enhancing a company's environmental credentials and meeting consumer demand for eco-friendly products, especially in food-packaging. The use of bio-derived AuNPs ensures that materials in contact with food are safe and minimize chemical leaching, addressing consumer safety and regulatory concerns.

CRediT authorship contribution statement

Maria Assunta Acquavia: Writing – review & editing, Writing – original draft, Visualization, Methodology, Investigation, Formal analysis, Data curation, Conceptualization. **Jennifer Gubitosa:** Writing – original draft, Investigation. **Vito Rizzi:** Writing – original draft, Investigation. **Pinalysa Cosma:** Writing – original draft, Visualization. **Carmine Gaeta:** Data curation. **Patrizia Iannece:** Writing – original draft. **Paolo Della Sala:** Writing – original draft, Data curation. **Antonio Guerrieri:** Writing – original draft. **Carmen Tesoro:** Writing – original draft. **Rosanna Ciriello:** Writing – original draft. **Filomena Lelario:** Writing – original draft. **Emanuela Gregori:** Writing – original draft, Visualization. **Paola Montoro:** Writing – original draft, Visualization. **Angela Di Capua:** Writing – original draft, Investigation, Data curation. **Giuliana Bianco:** Writing – review & editing, Supervision, Methodology, Conceptualization.

Declaration of competing interest

The authors declare that they have no known competing financial interests or personal relationships that could have appeared to influence the work reported in this paper.

Appendix A. Supplementary data

Supplementary data to this article can be found online at https://doi.org/10.1016/j.foodchem.2025.143427.

Data availability

Data will be made available on request.

References

Abid, M., Yaich, H., Cheikhrouhou, S., Khemakhem, I., Bouaziz, M., Attia, H., & Ayadi, M. A. (2017). Antioxidant properties and phenolic profile characterization by LC–MS/MS of selected Tunisian pomegranate peels. *Journal of Food Science and Technology, 54*(9), 2890–2901. https://doi.org/10.1007/s13197-017-2727-0

Acquavia, M. A., Pascale, R., Pappalardo, I., Santarsiero, A., Martelli, G., & Bianco, G. (2021). Characterization of quercetin derivatives in crossing combination of habanero white and capsicum annuum peppers and of anti-inflammatory and cytotoxic activity. *Separations, 8*(7). https://doi.org/10.3390/separations8070090

Ahmad, T., Bustam, M. A., Irfan, M., Moniruzzaman, M., Asghar, H. M. A., & Bhattacharjee, S. (2019). Mechanistic investigation of phytochemicals involved in green synthesis of gold nanoparticles using aqueous Elaeis guineensis leaves extract: Role of phenolic compounds and flavonoids. *Biotechnology and Applied Biochemistry, 66*(4), 698–708. https://doi.org/10.1002/bab.1787

Akhtar, S., Ismail, T., Fraternale, D., & Sestili, P. (2015). Pomegranate peel and peel extracts: Chemistry and food features. *Food Chemistry, 174*, 417–425. https://doi.org/10.1016/j.foodchem.2014.11.035

Alegria, E. C. B. A., Ribeiro, A. P. C., Mendes, M., Ferraria, A. M., Botelho Do Rego, A. M., & Pombeiro, A. J. L. (2018). Effect of phenolic compounds on the synthesis of gold nanoparticles and its catalytic activity in the reduction of nitro compounds. *Nanomaterials, 8*(5), 6–10. https://doi.org/10.3390/nano8050320

Allabashi, R., Stach, W., De La Escosura-Muñiz, A., Liste-Calleja, L., & Merkoçi, A. (2009). ICP-MS: A powerful technique for quantitative determination of gold nanoparticles without previous dissolving. *Journal of Nanoparticle Research, 11*(8), 2003–2011. https://doi.org/10.1007/s11051-008-9561-2

Amini, S. M., & Akbari, A. (2019). Metal nanoparticles synthesis through natural phenolic acids. *IET Nanobiotechnology, 13*(8), 771–777. https://doi.org/10.1049/iet-nbt.2018.5386

Arakawa, R., Yamaguchi, M., Hotta, H., Osakai, T., & Kimoto, T. (2004). Product analysis of caffeic acid oxidation by on-line electrochemistry/ electrospray ionization mass spectrometry. *Journal of the American Society for Mass Spectrometry, 15*(8), 1228–1236. https://doi.org/10.1016/j.jasms.2004.05.007

Brenton, A. G., & Godfrey, A. R. (2010). Accurate mass measurement: Terminology and treatment of data. *Journal of the American Society for Mass Spectrometry, 21*(11), 1821–1835. https://doi.org/10.1016/j.jasms.2010.06.006

Çam, M., & Hişil, Y. (2010). Pressurised water extraction of polyphenols from pomegranate peels. *Food Chemistry, 123*(3), 878–885. https://doi.org/10.1016/j.foodchem.2010.05.011

Chen, T. H., Yu, C. J., & Tseng, W. L. (2014). Sinapinic acid-directed synthesis of gold nanoclusters and their application to quantitative matrix-assisted laser desorption/ ionization mass spectrometry. *Nanoscale, 6*(3), 1347–1353. https://doi.org/10.1039/c3nr04991d

Daniel, M. C., & Astruc, D. (2004). Gold nanoparticles: Assembly, supramolecular chemistry, quantum-size-related properties, and applications toward biology, catalysis, and nanotechnology. *Chemical Reviews, 104*(1), 293–346. https://doi.org/10.1021/cr030698+

Dash, S. S., & Bag, B. G. (2014). Synthesis of gold nanoparticles using renewable Punica granatum juice and study of its catalytic activity. *Applied Nanoscience (Switzerland), 4*(1), 55–59. https://doi.org/10.1007/s13204-012-0179-4

Díaz-Mula, H. M., Tomás-Barberán, F. A., & García-Villalba, R. (2019). Pomegranate fruit and juice (cv. Mollar), rich in Ellagitannins and anthocyanins, also provide a significant content of a wide range of Proanthocyanidins. *Journal of Agricultural and Food Chemistry, 67*(33), 9160–9167. https://doi.org/10.1021/acs.jafc.8b07155

EL-Aguel, A., Pennisi, R., Smeriglio, A., Kallel, I., Tamburello, M. P., D'Arrigo, M., … Sciortino, M. T. (2022). Punica granatum Peel and leaf extracts as promising strategies for HSV-1 treatment. *Viruses, 14*(12). https://doi.org/10.3390/v14122639

Enomoto, H. (2021). Unique distribution of ellagitannins in ripe strawberry fruit revealed by mass spectrometry imaging. *Current Research in Food Science, 4*(June), 821–828. https://doi.org/10.1016/j.crfs.2021.11.006

Firuzi, O., Lacanna, A., Petrucci, R., Marrosu, G., & Saso, L. (2005). Evaluation of the antioxidant activity of flavonoids by "ferric reducing antioxidant power" assay and cyclic voltammetry. *Biochimica et Biophysica Acta - General Subjects, 1721*(1–3), 174–184. https://doi.org/10.1016/j.bbagen.2004.11.001

Fischer, U. A., Carle, R., & Kammerer, D. R. (2011). Identification and quantification of phenolic compounds from pomegranate (Punica granatum L.) peel, mesocarp, aril and differently produced juices by HPLC-DAD-ESI/MSn. *Food Chemistry, 127*(2), 807–821. https://doi.org/10.1016/j.foodchem.2010.12.156

Gubitosa, J., Rizzi, V., Fini, P., Del Sole, R., Lopedota, A., Laquintana, V., Denora, N., Agostiano, A., & Cosma, P. (2020). Multifunctional green synthetized gold nanoparticles/chitosan/ellagic acid self-assembly: Antioxidant, sun filter and tyrosinase-inhibitor properties. *Materials Science and Engineering C, 106*(July 2019), Article 110170. https://doi.org/10.1016/j.msec.2019.110170

Gubitosa, J., Rizzi, V., Lopedota, A., Fini, P., Laurenzana, A., Fibbi, G., Fanelli, F., Petrella, A., Laquintana, V., Denora, N., Comparelli, R., & Cosma, P. (2018). One pot environmental friendly synthesis of gold nanoparticles using Punica Granatum juice: A novel antioxidant agent for future dermatological and cosmetic applications. *Journal of Colloid and Interface Science, 521*, 50–61. https://doi.org/10.1016/j.jcis.2018.02.069

Gubitosa, J., Rizzi, V., Maggi, F., Laurenzana, A., Caprioli, G., Anceschi, C., … Cosma, P. (2023). From kiwi Peels' "end-of-life" to gold nanoparticles: The upcycling of a waste. *BioNanoScience, 13*(4), 1703–1725. https://doi.org/10.1007/s12668-023-01179-x

Gubitosa, J., Rizzi, V., Marasciulo, C., Maggi, F., Caprioli, G., Mustafa, A. M., … Cosma, P. (2023). Realizing eco-friendly water-resistant sodium-alginate-based films blended with a polyphenolic aqueous extract from grape pomace waste for potential food packaging applications. *International Journal of Molecular Sciences, 24*(14). https://doi.org/10.3390/ijms241411462

Hegazi, N. M., El-Shamy, S., Fahmy, H., & Farag, M. A. (2021). Pomegranate juice as a super-food: A comprehensive review of its extraction, analysis, and quality assessment approaches. *Journal of Food Composition and Analysis, 97*(August 2020), Article 103773. https://doi.org/10.1016/j.jfca.2020.103773

Helfrich, A., & Bettmer, J. (2011). Analysis of gold nanoparticles using ICP-MS-based hyphenated and complementary ESI-MS techniques. *International Journal of Mass Spectrometry, 307*(1–3), 92–98. https://doi.org/10.1016/j.ijms.2011.01.010

Helfrich, A., Brüchert, W., & Bettmer, J. (2006). Size characterisation of au nanoparticles by ICP-MS coupling techniques. *Journal of Analytical Atomic Spectrometry, 21*(4), 431–434. https://doi.org/10.1039/b511705d

http://gnps.ucsd.edu. (2022). *Global natural products social molecular networking (GNPS). Doi: 10.3390/plants12233970*.

Kalaycıoğlu, Z., & Erim, F. B. (2017). Total phenolic contents, antioxidant activities, and bioactive ingredients of juices from pomegranate cultivars worldwide. *Food Chemistry, 221*, 496–507. https://doi.org/10.1016/j.foodchem.2016.10.084

Krueger, D. A. (2012). Composition of pomegranate juice. *Journal of AOAC International, 95*(1), 163–168. https://doi.org/10.5740/jaoacint.11-178

Kumari, P., & Meena, A. (2020). Green synthesis of gold nanoparticles from Lawsoniainermis and its catalytic activities following the Langmuir-Hinshelwood mechanism. *Colloids and Surfaces A: Physicochemical and Engineering Aspects, 606*(June), Article 125447. https://doi.org/10.1016/j.colsurfa.2020.125447

Laszakovits, J. R., & MacKay, A. A. (2022). Data-based chemical class regions for Van Krevelen diagrams. *Journal of the American Society for Mass Spectrometry, 33*(1), 198–202. https://doi.org/10.1021/jasms.1c00230

Lee, K. X., Shameli, K., Yew, Y. P., Teow, S. Y., Jahangirian, H., Rafiee-Moghaddam, R., & Webster, T. J. (2020). Recent developments in the facile bio-synthesis of gold nanoparticles (AuNPs) and their biomedical applications. *International Journal of Nanomedicine, 15*, 275–300. https://doi.org/10.2147/IJN.S233789

Lijia, X., Guo, J., Chen, Q. Q., Baoping, J., & Zhang, W. (2014). Quantitation of phlorizin and phloretin using an ultra high performance liquid chromatography-electrospray ionization tandem mass spectrometric method. *Journal of Chromatography B: Analytical Technologies in the Biomedical and Life Sciences, 960*, 67–72. https://doi.org/10.1016/j.jchromb.2014.04.007

Ma, Y. L., Li, Q. M., Van Den Heuvel, H., & Claeys, M. (1997). Characterization of flavone and flavonol aglycones by collision-induced dissociation tandem mass spectrometry. *Rapid Communications in Mass Spectrometry, 11*(12), 1357–1364. https://doi.org/10.1002/(SICI)1097-0231(199708)11:12<1357::AID-RCM983>3.0.CO;2-9

Man, G., Xu, L., Wang, Y., Liao, X., & Xu, Z. (2022). Profiling phenolic composition in pomegranate Peel from nine selected cultivars using UHPLC-QTOF-MS and UPLC-QQQ-MS. *Frontiers in Nutrition, 8*(January), 1–12. https://doi.org/10.3389/fnut.2021.807447

Maphetu, N., Unuofin, J. O., Masuku, N. P., Olisah, C., & Lebelo, S. L. (2022). Medicinal uses, pharmacological activities, phytochemistry, and the molecular mechanisms of Punica granatum L. (pomegranate) plant extracts: A review. *Biomedicine and Pharmacotherapy, 153*(April), Article 113256. https://doi.org/10.1016/j.biopha.2022.113256

Mena, P., Calani, L., Dall'Asta, C., Galaverna, G., García-Viguera, C., Bruni, R., Crozier, A., & del Rio, D. (2012). Rapid and comprehensive evaluation of (poly) phenolic compounds in pomegranate (Punica granatum L.) juice by UHPLC-MSn. *Molecules, 17*(12), 14821–14840. https://doi.org/10.3390/molecules171214821

Moini, M., Jones, B. L., Rogers, R. M., & Jiang, L. (1998). Sodium trifluoroacetate as a tune/calibration compound for positive- and negative-ion electrospray ionization mass spectrometry in the mass range of 100-4000 Da. *Journal of the American Society for Mass Spectrometry, 9*(9), 977–980. https://doi.org/10.1016/S1044-0305(98)00079-8

Montefusco, A., Durante, M., Migoni, D., De Caroli, M., Ilahy, R., Pék, Z., … Lenucci, M. S. (2021). Analysis of the phytochemical composition of pomegranate fruit juices, peels and kernels: A comparative study on four cultivars grown in southern Italy. *Plants, 10*(11), 1–23. https://doi.org/10.3390/plants10112521

Nicolardi, S., Van Der Burgt, Y. E. M., Codée, J. D. C., Wuhrer, M., Hokke, C. H., & Chiodo, F. (2017). Structural characterization of biofunctionalized gold nanoparticles by ultrahigh-resolution mass spectrometry. *ACS Nano, 11*(8), 8257–8264. https://doi.org/10.1021/acsnano.7b03402

Onzo, A., Acquavia, M. A., Cataldi, T. R. I., Ligonzo, M., Coviello, D., Pascale, R., … Bianco, G. (2020). Coceth sulfate characterization by electrospray ionization tandem mass spectrometry. *Rapid Communications in Mass Spectrometry, 34*(20), 1–10. https://doi.org/10.1002/rcm.8884

Onzo, A., Acquavia, M. A., Pascale, R., Iannece, P., Gaeta, C., Lelario, F., … Di Capua, A. (2022). Untargeted metabolomic analysis by ultra-high-resolution mass spectrometry for the profiling of new Italian wine varieties. *Analytical and Bioanalytical Chemistry, 7805–7812*. https://doi.org/10.1007/s00216-022-04314-x

Onzo, A., Pascale, R., Acquavia, M. A., Cosma, P., Gubitosa, J., Gaeta, C., … Bianco, G. (2021). Untargeted analysis of pure snail slime and snail slime-induced au nanoparticles metabolome with MALDI FT-ICR MS. *Journal of Mass Spectrometry, 56*(5). https://doi.org/10.1002/jms.4722

Paidari, S., & Ibrahim, S. A. (2021). Potential application of gold nanoparticles in food packaging: A mini review. *Gold Bulletin, 54*(1), 31–36. https://doi.org/10.1007/s13404-021-00290-9

Pala, Ç. U., & Toklucu, A. K. (2011). Effect of UV-C light on anthocyanin content and other quality parameters of pomegranate juice. *Journal of Food Composition and Analysis, 24*(6), 790–795. https://doi.org/10.1016/j.jfca.2011.01.003

Panda, B. R., & Chattopadhyay, A. (2007). Synthesis of au nanoparticles at "all" pH by H2O2 reduction of HAuCl4. *Ournal of Nanoscience and Nanotechnology, 7*(6), 1911-1915(5).

Parashar, A. (2010). Lipid content and fatty acid composition of seed oils from six pomegranate cultivars. *International Journal of Fruit Science, 10*(4), 425–430. https://doi.org/10.1080/15538362.2010.530129

Parveen, K., Banse, V., & Ledwani, L. (2016). Green synthesis of nanoparticles: Their advantages and disadvantages. *AIP Conference Proceedings, 1724*(January 1973). https://doi.org/10.1063/1.4945168

Pascale, R., Acquavia, M. A., Onzo, A., Cataldi, T. R. I., Calvano, C. D., & Bianco, G. (2021). *Analysis of surfactants by mass spectrometry: Coming to grips with their diversity* (pp. 1–32). June: Mass Spectrometry Reviews. https://doi.org/10.1002/mas.21735

Pascale, R., Bianco, G., Cataldi, T. R. I., Kopplin, P. S., Bosco, F., Vignola, L., … Milella, L. (2018). Mass spectrometry-based phytochemical screening for hypoglycemic activity of Fagioli di Sarconi beans (Phaseolus vulgaris L.). *Food Chemistry, 242*(June 2017), 497–504. https://doi.org/10.1016/j.foodchem.2017.09.091

Passamonti, S., Vrhovsek, U., Vanzo, A., & Mattivi, F. (2003). The stomach as a site for anthocyanins absorption from food. *FEBS Letters, 544*(1–3), 210–213. https://doi.org/10.1016/S0014-5793(03)00504-0

Pavlov, J., & Attygalle, A. B. (2019). Gold nanoparticles (AuNPs) as reactive matrix for detection of trace levels of HCN in air by laser desorption/ionization mass spectrometry (LDI-MS). *Journal of the American Society for Mass Spectrometry, 30*(5), 806–813. https://doi.org/10.1007/s13361-018-02131-0

Pradeep, M., Kruszka, D., Kachlicki, P., Mondal, D., & Franklin, G. (2022). Uncovering the phytochemical basis and the mechanism of plant extract-mediated eco-friendly synthesis of silver nanoparticles using ultra-performance liquid chromatography coupled with a photodiode Array and high-resolution mass spectrometry. *ACS Sustainable Chemistry and Engineering, 10*(1), 562–571. https://doi.org/10.1021/acssuschemeng.1c06960

Qian, K., Rodgers, R. P., Hendrickson, C. L., Hughey, C. A., & Marshall, A. G. (2002). Kendrick mass defect spectrum: A compact visual analysis for ultrahigh-resolution broadband mass spectra. *Analytical Chemistry, 73*(19), 4676–4681. https://doi.org/10.1021/ac010560w

Qu, W., Breksa, A. P., Pan, Z., & Ma, H. (2012). Quantitative determination of major polyphenol constituents in pomegranate products. *Food Chemistry, 132*(3), 1585–1591. https://doi.org/10.1016/j.foodchem.2011.11.106

Ramirez, J. E., Zambrano, R., Sepúlveda, B., & Simirgiotis, M. J. (2014). Antioxidant properties and hyphenated HPLC-PDA-MS profiling of chilean pica mango fruits (Mangifera indica L. Cv. piqueño). *Molecules, 19*(1), 438–458. https://doi.org/10.3390/molecules19010438

Raveendran, P., Fu, J., & Wallen, S. L. (2003). Completely "green" synthesis and stabilization of metal nanoparticles. *Journal of the American Chemical Society, 125*(46), 13940–13941. https://doi.org/10.1021/ja029267j

Regos, I., Urbanella, A., & Treutter, D. (2009). Identification and quantification of phenolic compounds from the forage legume sainfoin (Onobrychis viciifolia). *Journal of Agricultural and Food Chemistry, 57*(13), 5843–5852. https://doi.org/10.1021/jf900625r

Saleemi, M. A., Alallam, B., Yong, Y. K., & Lim, V. (2022). Synthesis of zinc oxide nanoparticles with bioflavonoid Rutin: Characterisation, antioxidant and antimicrobial activities and in vivo cytotoxic effects on Artemia Nauplii. *Antioxidants, 11*(10). https://doi.org/10.3390/antiox11101853

Salek, R. M., Steinbeck, C., Viant, M. R., Goodacre, R., & Dunn, W. B. (2013). The role of reporting standards for metabolite annotation and identification in metabolomic studies. *GigaScience, 2*(1), 2–4. https://doi.org/10.1186/2047-217X-2-13

Sentandreu, E., Cerdán-Calero, M., & Sendra, J. M. (2013). Phenolic profile characterization of pomegranate (Punica granatum) juice by high-performance liquid chromatography with diode array detection coupled to an electrospray ion trap mass analyzer. *Journal of Food Composition and Analysis, 30*(1), 32–40. https://doi.org/10.1016/j.jfca.2013.01.003

Shervani, Z., & Yamamoto, Y. (2011). Carbohydrate-directed synthesis of silver and gold nanoparticles: Effect of the structure of carbohydrates and reducing agents on the size and morphology of the composites. *Carbohydrate Research, 346*(5), 651–658. https://doi.org/10.1016/j.carres.2011.01.020

Singh, B., Singh, J. P., Kaur, A., & Singh, N. (2018). Phenolic compounds as beneficial phytochemicals in pomegranate (Punica granatum L.) peel: A review. *Food Chemistry, 261*(December 2017), 75–86. https://doi.org/10.1016/j.foodchem.2018.04.039

Spáčil, Z., Nováková, L., & Solich, P. (2008). Analysis of phenolic compounds by high performance liquid chromatography and ultra performance liquid chromatography. *Talanta, 76*(1), 189–199. https://doi.org/10.1016/j.talanta.2008.02.021

Spano, M., Maccelli, A., di Matteo, G., Ingallina, C., Biava, M., Crestoni, M. E., … Mannina, L. (2021). Metabolomic profiling of fresh goji (Lycium barbarum l.) berries from two cultivars grown in Central Italy: A multi-methodological approach. *Molecules, 26*(17), 1–23. https://doi.org/10.3390/molecules26175412

Tandiana, R., Sicard-Roselli, C., Van-Oanh, N. T., Steinmann, S., & Clavaguéra, C. (2022). In-depth theoretical understanding of the chemical interaction of aromatic compounds with a gold nanoparticle. *Physical Chemistry Chemical Physics, 24*(41), 25327–25336. https://doi.org/10.1039/d2cp02654f

Van Elswijk, D. A., Schobel, U. P., Lansky, E. P., Irth, H., & Van Der Greef, J. (2004). Rapid dereplication of estrogenic compounds in pomegranate (Punica granatum) using on-line biochemical detection coupled to mass spectrometry. *Phytochemistry, 65*(2), 233–241. https://doi.org/10.1016/j.phytochem.2003.07.001

Ventura, G., Bianco, M., Calvano, C. D., Bianco, G., Di Capua, A., Coniglio, D., … Cataldi, T. R. I. (2024). Mass spectrometric characterization of aminophospholipids containing N-(2-hydroxyethyl)glycine in kombu algae extracts. *Rapid Communications in Mass Spectrometry, 38*(17), 1–11. https://doi.org/10.1002/rcm.9843

Vernon Singleton Rudolf Orthofer, R. L.-R. (1999). Analysis of Total phenols and other oxidation substrates and antioxidants by means of Folin-Ciocalteu reagent. *Methods in Enzymology, 299*, 152–178. https://doi.org/10.1016/j.scienta.2016.11.004

Weinberg, H., Galyean, A., & Leopold, M. (2011). Evaluating engineered nanoparticles in natural waters. *TrAC - Trends in Analytical Chemistry, 30*(1), 72–83. https://doi.org/10.1016/j.trac.2010.09.006

Ying, S., Guan, Z., Ofoegbu, P. C., Clubb, P., Rico, C., He, F., & Hong, J. (2022). Green synthesis of nanoparticles: Current developments and limitations. *Environmental Technology and Innovation, 26*, Article 102336. https://doi.org/10.1016/j.eti.2022.102336

Zengru, W., Gao, W., Phelps, M. A., Di, W., Miller, D. D., & J. T. D.. (2004). Favorable effects of weak acids on negative-ion electrospray ionization mass spectrometry. *Analytical Chemistry, 76*(3), 839–847.

Zhang, Y., Wang, D., Lee, R. P., Henning, S. M., & Heber, D. (2009). Absence of pomegranate ellagitannins in the majority of commercial pomegranate extracts: Implications for standardization and quality control. *Journal of Agricultural and Food Chemistry, 57*(16), 7395–7400. https://doi.org/10.1021/jf9010017

Zhou, Y., Kong, Y., Kundu, S., Cirillo, J. D., & Liang, H. (2012). Antibacterial activities of gold and silver nanoparticles against Escherichia coli and bacillus Calmette-Guérin. *Journal of Nanobiotechnology, 10*, 1–9. https://doi.org/10.1186/1477-3155-10-19